nagra.

ARBEITSBERICHT NAB 24-10 Rev. 1

Geological Properties of the Jura Ost, Nördlich Lägern and Zürich Nordost Siting Regions for Safety Assessment

November 2024

Nagra | National Cooperative for the Disposal of Radioactive Waste
Hardstrasse 73 | 5430 Wettingen | Switzerland
+41 56 437 11 11 | info@nagra.ch | nagra.ch

nagra.

ARBEITSBERICHT NAB 24-10 Rev. 1

Geological Properties of the Jura Ost, Nördlich Lägern and Zürich Nordost Siting Regions for Safety Assessment

November 2024

KEYWORDS
Geological abstraction, 3D surfaces, depth maps, thickness maps, parameter bandwidth, mineralogy, porosity, hydraulic conductivity, hydraulic head, hydraulic gradient, geomechanical properties

Nagra | **National Cooperative for the Disposal of Radioactive Waste**
Hardstrasse 73 | 5430 Wettingen | Switzerland
+41 56 437 11 11 | info@nagra.ch | nagra.ch

Nagra Arbeitsberichte ("Working Reports") present the results of work in progress that have not necessarily been subject to a comprehensive review. They are intended to provide rapid dissemination of current information.

Main authors: D. Arndt, J. Becker, G. Deplazes, S. Giger & N. Roy

Contributions: D. Carraro, M. Claps, E. Crisci[1], M. Schnellmann & D. Traber

Editorial work and graphical support: P. Blaser, L. Gregorczyk, B. Habermacher, F. Maier & M. Unger

[1] Nesol - Numerical Engineering Solutions

This report has benefited from numerous technical discussions and reviews by various people inside and outside Nagra. We would like to thank these people and all others who contributed to the preparation of this report.

NAB 24-10, Mai 2025: Corrigendum

This report was revised in May 2025. References in all chapters were clarified and supplemented. Furthermore, a few formulations in Chapters 3.3 and 5.3.5 were clarified and the axis labelling in Figures 5.1 to 5.3 was corrected. Finally, Enclosure 3-5c has been replaced (in the 1st version this was incorrectly a copy of Enclosure 3-4c)

To maintain consistency with the documents submitted for the general licence applications, the original publication date is retained.

Abstract

The Sectoral Plan for Deep Geological Repositories (SGT) has defined the safety-oriented site selection process since 2008. In the third and final stage of the site selection process, the database for the geological site characterisation was improved significantly in the three siting regions Jura Ost (JO), Nördlich Lägern (NL) and Zürich Nordost (ZNO).

Compared to SGT Stage 2, core observations, geophysical logging, and in-situ and laboratory testing were expanded significantly with nine new exploration boreholes (TBO). The regional 3D-seismic measurements in the siting regions also represent an important new dataset. Overall, the combined exploration efforts with 3D seismics and deep boreholes ensures a comparable data basis for all the siting regions.

This report focuses on the spatial geometry of geological layers and key rock properties relevant for transport and assessment of barrier integrity. These properties are evaluated in mineralogical and petrophysical, hydrogeological and geomechanical chapters. The derivation of representative parameter ranges for these key properties is based on a data-driven abstraction and subdivision of the geological units. The observations and measurements of the TBO are compiled and interpreted considering spatial variability, scaling aspects and uncertainties. Representative parameter value ranges are specified for each of the three siting regions.

The report complements the geosynthesis (Nagra 2024e) with a comprehensive site-specific geological description and parametrisation, which serve as a basis for the repository performance assessment (Nagra 2024g) and radiological consequence analysis (Nagra 2024i).

Table of Contents

List of Tables

List of Figures

List of Enclosures

Note: All Enclosures are included in the digital version of this report and can be found under the paper clip symbol.
In the printed version the Enclosures 2-2a-c, 2-3a-c und 5-1a-c are at the end of the report.
All other Enclosures are only included in the digital version.

1 Introduction

1.1 Aims of the report

This report provides a quantitative geological description of the potential repository zone in the Jura Ost (JO), Nördlich Lägern (NL) and Zürich Nordost (ZNO) siting regions and complements the geosynthesis report (Nagra 2024e). While the geosynthesis highlights similarities and differences between the siting regions and discusses the key geological processes, this report focuses on a local geological characterisation of the central areas of the three siting regions, the area of interest (AOI), as a quantitative basis for numerical modelling of repository performance assessments (Nagra 2024k) and radiological consequence analysis (Nagra 2024i).

More specifically, the report covers the following aspects for the three siting regions:

- Abstraction of geological, stratigraphic units as a basis for modelling purposes in performance assessment and safety analysis, hereafter referred to simply as "abstracted units"
- Geometry of the abstracted units in the potential repository zones (local "layer cake models")
- Key properties of the abstracted units (e.g. mineralogy, hydraulic properties), including explanation of database, assumptions and concepts used to constrain parameter bandwidths

Geological models and properties are being used in a variety of scoping calculations and modelling approaches, depending on the goals and focus of the investigation. It is therefore challenging to provide global parameter values, but those specified in the enclosures should be considered as a basis for calculations and further analyses.

The model horizons in this report focus on a perimeter which contains only few seismically mappable faults, without major throws. Structural maps are therefore not presented here but can be found in Section 4.3.4 of Nagra (2024e) as well as in Section 5.3 of Nagra (2024a, 2024b, 2024c). The following aspects of the description of the geosphere are neither covered in this report, nor in the geosynthesis (Nagra 2024e):

- The engineering geological characterisation of the three siting regions relevant for construction planning and construction risk analyses are covered in Nagra (2023a, 2023b, 2023c). Specific geomechanical parameters of Opalinus Clay used for construction design and tunnel-static analyses are specified in Section 3.3.1 of Nagra (2023d)
- A detailed evaluation of the site-specific stress field is provided in Nagra (2024j), including estimates of depth-dependent stress magnitudes in Opalinus Clay (Chapter 5.1) and in overlying formations along potential access structures (Appendix I).
- Diffusion properties of host rock and confining units are described in Chapter 6 of Glaus et al. (2024).
- Sorption properties of host rock and confining units are quantified in Chapter 5 of Miron et al. (2024).
- For thermal properties and temperature conditions see Chapter 2 & App. A of Nagra (2024l).
- Specific parameters relevant for the assessments of the effect of the future repository evolution on the geological barrier function (e.g. Excavation Damage Zone evolution, gas transport properties, temperature effects) are covered in the Appendix of Nagra (2024k).
- The porewater chemistry of Opalinus Clay which is a constraint for the transport of radionuclides (speciation, solubility, sorption, diffusion) and for the assessment of the geochemical stability of the engineered barriers is documented in Chapter 5 of Mäder & Wersin (2023).

1.2 Structure of the report

The main products of the report are represented in an extensive appendix:

- Encl. 2 to 6 visualise the site-specific abstracted units (lateral extent and parameter ranges)
- Encl. 7 includes a listing of the recommended parameter ranges

The text provides topic-specific background to understand the content of these enclosures and generally includes a description of the input data and of the used concepts and methods for abstraction and parametrisation:

- In Chapter 2 the abstraction of the stratigraphic column to units with similar properties is described.
- Chapter 2 introduces the local 3D model describing the geometry of these abstracted units.
- Chapters 4 to 6 are concerned with the basic, hydraulic, and mechanical properties of the abstracted units:
  - Chapter 4: mineralogy and basic rock properties
  - Chapter 4: hydrogeology (conductivities, heads and gradients)
  - Chapter 5: geomechanical properties
- Chapter 7 summarises the key points of the report.

1.3 Database

Most input data are documented in the borehole-specific data reports (Tab. 1-1). The continuous mineralogy and porosity profiles used in this report are based on a re-analysis after the TBO campaign applying a harmonised and refined approach (Becker & Marnat 2024). The seismic horizon and fault interpretations are documented in site-specific seismic interpretation reports (JO: Nagra 2024a, NL: Nagra 2024b, ZNO: Nagra 2024c). Additional data sources are cited in the individual sections.

Tab. 1-1: List of new deep boreholes (TBO) drilled 2019 – 2022 and associated data reports

MD: Measured depth below ground level. * Deviated borehole, true vertical depth 745.33 m.

Siting region	**TBO Name**	**Abbreviation used in report**	**Data reports**	**Nagra NAB No.**	**Final depth** [m MD]
JO	Bözberg-1-1	BOZ1	Nagra (ed.) 2022a	NAB 21-21	1'037.39
JO	Bözberg-2-1	BOZ2	Nagra (ed.) 2022b	NAB 21-22	829.11
NL	Bülach-1-1	BUL1	Nagra (ed.) 2021a	NAB 20-08	1'370.19
NL	Stadel-3-1	STA3	Nagra (ed.) 2022d	NAB 22-01	1'280.88
NL	Stadel-2-1	STA2	Nagra (ed.) 2022c	NAB 22-02	1'288.12
NL	Bachs-1-1	BAC1	Nagra (ed.) 2023a	NAB 22-04	1'306.26
ZNO	Trüllikon-1-1	TRU1	Nagra (ed.) 2021c	NAB 20-09	1'310.0
ZNO	Marthalen-1-1	MAR1	Nagra (ed.) 2021b	NAB 21-20	1'099.25
ZNO	Rheinau-1-1	RHE1	Nagra (ed.) 2023b	NAB 22-03	827.99*

2 Stratigraphic overview and abstraction

2.1 Introduction

The stratigraphic abstraction aims to divide the interval of the host rock and its low permeability confining units into units with similar characteristics regarding key parameters for performance assessment and radiological consequences analysis. The relevant interval between the main aquifers is defined in JO from the top of the Muschelkalk Group to the base of the interfingering of the Hauptrogenstein and the Klingnau Formation. In NL and ZNO the relevant section is defined from the top of the Muschelkalk Group to the base of the Villigen Formation (Top Wildegg Formation, within Malm Group). Therefore, the relevant section is delimited by the aquifers of the Muschelkalk Group, Dogger Group (Hauptrogenstein) and Malm Group.

2.2 Database and Methodology

The abstracted units represent units with similar transport properties. In Stage 2 of the Sectoral Plan for Deep Geological Repositories (SGT Stage 2), these stratigraphic units were mainly delimited based on the clay-mineral content (Nagra 2014a, Chapter 4, see also Dossier IV of the TBO reports as indicated in Tab. 1-1) measured in few boreholes (mainly Riniken, Weiach and Benken). In the current investigation phase, the database has been improved considerably with new boreholes and improved quantitative log analysis (referred to as “MultiMin”; Becker & Marnat 2024). The abstraction presented in this report is mainly defined according to mineralogy traced by MultiMin (Encl. 2-2a to 2-2c).

The boundaries of the abstracted units were set by integrating different stratigraphic analyses. Lithostratigraphic boundaries in core and log depth of deep boreholes relevant for the three siting regions were defined in individual data reports (Tab. 1-1). The tops of the lithostratigraphic units in metres measured depth (m MD) can be found in the columns “RBG Lithostratigraphy, Core Depth” and “RBG Lithostratigraphy, Log Depth” in the Encl. 2-4b to d. After finishing these data reports, the core-to-log depth conversion has been revised partly. Additionally, petrophysical logs were re-assessed and some lithostratigraphic boundaries were adjusted to integrate all presented borehole data, such as borehole images, wireline logs, core photos, and core descriptions. The resulting lithostratigraphic boundaries can be found in the columns “RBG Lithostratigraphy, Revised Log Depth” in the Encl. 2-4b to d. The lithostratigraphic tops as listed in columns “RBG Lithostratigraphy, Core Depth” and “RBG Lithostratigraphy, Revised Log Depth” are considered as reference for reporting in the framework of the general licence application, “RBG Litho-stratigraphy, Log Depth” was dismissed. But it is highlighted that differences between “RBG Lithostratigraphy, Log Depth” and “RBG Lithostratigraphy, Revised Log Depth” are generally very small (typically <50 cm). Depths with larger differences (i.e. >50 cm) are commented in Encl. 2-4b to d (refer to column “Comments”).

In a next step the records of lithostratigraphy, biostratigraphy and sequence stratigraphy were integrated, and a new chronostratigraphic framework was established. This chronostratigraphic framework comprises the interpretation of timelines, i.e. horizons that represent the same time in different boreholes. These timelines show a smaller or larger uncertainty depending on the available data and depositional environment. The relative position of timelines to lithostra-tigraphic boundaries can be found in Encl. 2-4a, sheet “Stratigraphic Framework”. Many timelines follow or are closely related to major lithostratigraphic boundaries. The depth of timelines in metres Measured Depth are listed in the column “RBG Timelines Log Depth” in the Encl. 2-4b to d. This new chronostratigraphic framework enables a temporal analysis of the facies distribution and depositional environment. The timelines also define reference horizons in the

interpretation of the 3D-seismic cube, as seismic reflectors generally follow timelines (Vail et al. 1977, Eberli et al. 2002). More information on the timelines can be found in Chapter 4 of Nagra (2024e).

The boundaries of the abstracted units are also defined based on timelines (Encl. 2-1a to 2-1c, column "RBG Abstracted Units for Safety Analysis" in Encl. 2-4b to d). A selection of timelines has been picked in the 3D-seismic cube (Nagra 2024a, 2024b, 2024c), so individuals or groups of abstracted units can be traced in three dimensions (Chapter 2). An overview of the top and thickness of the abstracted units per borehole and siting region can be found in sheets 2_1 and 2_2 of Encl. 7-1.

2.3 Results: Definition of abstracted units for safety analysis with similar properties

From deeper/older to shallower/younger, the following abstracted units can be distinguished (Encl. 2-3a to 2-3c):

- The **Bänkerjoch Formation** (Time interval *237_Lad_400_Top_Muschelkalk_Gr* to *227_Car_300_Top_Baenkerjoch_Fm*) is divided into the three units Dolomitic-Anhydritic Keuper (**DAK**), Massive Anhydritic Keuper (**MAK**) and Anhydritic-Argillaceous Keuper (**AAK**). The massive anhydritic interval towards the base of the Bänkerjoch Formation was delimited as its very high content in anhydrite and low content of other components could be relevant for diffusive transport (low diffusion coefficients of anhydrite and indications from natural tracer profiles).
- The **Klettgau Formation** is divided into several units over all three siting regions. This relatively high degree of detail in the Klettgau Formation reflects the variability in its characteristics. This variability traces the originally diverse terrestrial to partly marine depositional environments and the consecutive diagenesis. The different sedimentological and hydrogeological characteristics of the Klettgau Formation in the siting regions is relevant for site comparison – this warrants the comparably large number of subunits.
- In the **Ergolz Member** (Time interval *227_Car_300_Top_Baenkerjoch_Fm* to *227_Car_200_Top_Ergolz_Mb*), the lowermost Member of the Klettgau Formation, two different abstracted units are distinguished. The first unit, the Argillaceous Keuper (**AK1**), represents the clay-mineral-rich intervals that were originally deposited as fluvial floodplain deposits. The second unit, the Sandy Keuper (**SK**), represents the quartz-/feldspar-rich intervals that were originally deposited in fluvial channels. The SK unit can be traced by high quartz/feldspar (mineral contents of >50%, Section 4.3.2). According to this fluvial depositional environment, SK occurs in a complicated channel network that is interbedded in the floodplain deposits of AK1. This is indicated in Encl. 2-3a to 2-3c by SK forming a lens that is embedded in AK1. Note that due to the complex depositional environment in a terrestrial fluvial system location and geometry of AK1 units are difficult to predict. The facies is expected to occur locally in all three siting regions.

- The overlying sequence of **Gansingen Member to Gruhalde Member** and the corresponding abstracted units differ between the geological siting regions.
  - In Jura Ost the Dolomitic Keuper (**JO-DK,** Time interval *227_Car_200_Top_Ergolz_Mb* to *227_Car_100_Top Gansingen_Mb*) stratigraphic unit is followed by the Argillaceous Keuper (**JO-AK2/3**, Time interval *227_Car_100_Top Gansingen_Mb* to *199.5_Het_100_Top_Schambelen_Mb*). The lowermost Member of the overlying Staffelegg Formation, the Schambelen Member, is also included in the JO-AK2/3 unit because of its relatively similar characteristics regarding transport. In Jura Ost the Seebi Member is not occurring or just as a thin layer (<1 m). In this sequence of JO the JO-DK unit should be highlighted as it is characterised by low clay-mineral contents and high dolomite contents. It is also thicker and has a higher macroporosity compared to Nördlich Lägern (in ZNO the Gansingen Member is anhydritic not dolomitic).
  - In Nördlich Lägern the Dolomitic Keuper and Argillaceous Keuper stratigraphic units alternate, i.e. **NL-DK1** (Gansingen Member, Time interval *227_Car_200_Top_Ergolz_Mb* to *227_Car_100_Top_Gansingen_Mb*), **NL-AK2** ("lower" Gruhalde Member, Time interval *227_Car_100_Top_Gansingen_Mb* to *208.5_Nor_200_Top_lw_Gruhalde_Mb*), **NL-DK2** (Seebi Member, Time interval *208.5_Nor_200_Top_lw_Gruhalde_Mb to 208.5_Nor_100_Top_Seebi_Mb*) and **NL-AK3** ("upper" Gruhalde Member of the Klettgau Formation and Schambelen Member of the Staffelegg Formation, Time interval *208.5_Nor_100_Top_Seebi_Mb* to *199.5_Het_100_Top_ Schambelen_Mb*).
  - In Zürich Nordost the Anhydritic Keuper (**ZNO-ANK**, Gansingen Member, Time interval *227_Car_200_Top_Ergolz_Mb* to *227_Car_100_Top_ Gansingen_Mb*) stratigraphic unit is followed by the Argillaceous Keuper (**ZNO-AK2** ("lower" Gruhalde Member, Time interval *227_Car_100_Top_Gansingen_Mb* to *208.5_Nor_200_ Top_lw_Gruhalde_Mb*), the Dolomitic-Sandy Keuper (**ZNO-DSK**, Seebi Member, Time interval *208.5_Nor_200_Top_lw_Gruhalde_Mb to 208.5_Nor_100_Top_Seebi_Mb*) and the Argillaceous Keuper (**ZNO-AK3**, "upper" Gruhalde Member of the Klettgau Formation and Schambelen Member of the Staffelegg Formation, Time interval *208.5_Nor_100_Top_Seebi_Mb* to *199.5_Het_100_Top_Schambelen_Mb*). In this sequence of ZNO the ZNO-DSK unit should be highlighted as it is characterised by low clay-mineral contents and high dolomitic (upper part) and sandy (lower part) contents. It also includes a higher macroporosity compared to NL.
- In the **Staffelegg Formation** three abstracted units are distinguished in the three geological siting regions. Firstly, the Calcareous Lias (**CL,** Time interval *199.5_Het_100_Top_Schambelen_Mb* to *192.9_Sin_200_Top_Beggingen_Mb*) corresponds to the Beggingen Member. A relatively thin layer with low clay-mineral contents and elevated calcareous contents. Secondly, the Argillaceous Lias (**AL,** Time interval *192.9_Sin_200_Top_Beggingen_Mb* to *192.9_Sin_100_Top_Frick_Mb*) corresponds to the Frick Member. It is characterised by high clay-mineral contents and low carbonate contents. Thirdly, the Marly Lias (**ML,** Time interval *192.9_Sin_100_Top_Frick_Mb* to *174.7_Toa_100_Top_Lias_Gr*) corresponds to the thin, condensed Grünschholz, Breitenmatt and Rickenbach Members, the Rietheim Member and the Gross Wolf Member. The Marly Lias is characterised by medium clay-mineral contents with lowest contents in the Grünschholz, Breitenmatt and Rickenbach Members.

- The **Opalinus Clay** is defined with one abstracted unit (**OPA,** time interval *174.4_Toa_100_Top_Lias_Gr* to *170.9_Aal_300_Top_Opalinus Clay*). It is characterised by high clay-mineral contents (>40%). The rest is dominated by quartz/feldspar and some calcite. In comparison to the other Mesozoic formations it shows low vertical and horizontal variability in its mineralogical characteristics.
- In the **Dogger Group above Opalinus Clay** follows a succession that shows more variability. The first part of the succession corresponds to the lower part of the Passwang Formation (up to top of the «Humphriesi-Schichten») in JO and the «Murchisonae-Oolith Formation», Wedelsandstein Formation and «Humphriesioolith Formation» in NL and ZNO. This succession is dominated by high clay-mineral contents. However, up to a few metres thick successions of more weathering-resistant "hard beds" occur intercalated in the clay-mineral-rich sedimentary rocks (Bläsi et al. 2013). Mainly based on their lithology, three types of "hard beds" can be generally distinguished (Nagra 2024e): 1) biomicritic limestone, 2) silty to sandy, bioclastic limestone, and 3) iron-oolite or iron-oolitic beds. In this succession two abstracted units are differentiated. The succession is dominated by the Sandy-Calcareous-Argillaceous Dogger unit (**SCAD,** *170.9_Aal_300_Top_Opalinus Clay* to *168.2_Baj_200_Top_Brueggli_Mb* (JO) resp. *168.2_Baj_300_Base_Herrenwis_Unit_eq* (NL) resp. *168.2_Baj_200_Intra_Humphriesioolith_Fm* (ZNO)). This unit corresponds to the intervals with elevated clay-mineral contents. The second unit, the Sandy-Calcareous Dogger unit (**SCD**) corresponds to the intervals with lower clay-mineral contents. To distinguish between SCAD and SCD units a clay-mineral content threshold value of 20 wt.% was applied (see Section 4.3.1 for more information).
- The overlying succession of the Dogger Group differs in the geological siting regions. In JO the succession is represented by the Calcareous-Argillaceous Dogger stratigraphic unit (**JO-CAD**, Time interval *168.2_Baj_200_Top_Brueggli_Mb* to *168.2_Baj_100_Top_Passwang_Fm*). It corresponds mostly to the Rothenfluh Member of the Passwang Formation that is characterised by medium clay-mineral contents. In NL four different stratigraphic units are differentiated. In the eastern part of Nördlich Lägern (STA3 and BUL1 boreholes) occurs the Calcareous Dogger stratigraphic unit (**NLE-CD**, Time interval *168.2_Baj_300_Base_Herrenwis_Unit_eq* to *168.2_Baj_200_Top_Herrenwis_Unit_eq*). It represents an isolated carbonate platform that is characterised by high calcareous contents. Its lateral extent within the area of interest can be mapped in the 3D-seismic cube (Chapter 4). It corresponds to the «Herrenwis Unit». Towards the west (STA2 and WEI boreholes) the NLE-CD is neighboured by the Calcareous Dogger stratigraphic unit (**NLW-CD**). It is characterised by elevated calcareous contents and thins from the platform towards the west. It corresponds to the time-equivalent, calcareous basinal part of the «Herrenwis Unit», the periplatform wedge. Its lateral extent within the area of interest can be approximated in the 3D-seismic cube (Chapter 4). Even further towards the west NLW-CD is neighboured by the Argillaceous Dogger stratigraphic unit (**NL-ARD**, BAC1 borehole). It represents the time-equivalent, silicilastic-rich basinal succession of the «Herrenwis Unit». It is characterised by elevated clay-mineral contents and is only several metres thick. These three stratigraphic units are overlain by the Argillaceous Dogger (**NL-AD and ZNO-AD**, Time interval *168.2_Baj_200_Top_Herrenwis_Unit_eq* to *154.8_Oxf_975_Top_Dogger_Gr*). It is characterised dominantly by high clay-mineral contents. The thickness is high in the east and diminishes over the carbonate platform, it seems to fill up the original topography. It represents the «Parkinsoni-Württembergica-Schichten», Variansmergel Formation and the iron-oolitic Wutach Formation. In ZNO the succession is represented by the Argillaceous Dogger stratigraphic unit (AD, Time interval *168.2_Baj_200_Intra_Humphriesioolith_Fm* to *154.8_Oxf_975_To_Dogger_Gr*). It is characterised dominantly by high clay-mineral contents. It also represents the «Parkinsoni-Württembergica-Schichten», Variansmergel Formation and the iron-oolitic Wutach Formation.

- In the Malm Group of NL two types of abstracted units are differentiated. The Marly Malm stratigraphic unit (**NL-MM1** & **NL-MM2**, *154.8_Oxf_975_Top_Dogger_Gr* to *154.8_Oxf_750_Intra_Wildegg_Fm* & *154.8_Oxf_700_nTop_Gerstenhuebel_Bd* to *154.8_Oxf_300_nTop_Wildegg_Fm*) is characterised by medium clay-mineral and calcareous contents. It represents the Birmenstorf Member and the calcareous marls of the Effingen Member of the Wildegg Formation. The Calcareous Malm stratigraphic unit (**NL-CM**, *154.8_Oxf_750_Intra_Wildegg_Fm* to *154.8_Oxf_700_nTop_Gerstenhuebel_Bd*) is characterised by high calcareous contents. It represents the interval with highest calcareous contents of the Effingen Member, mostly corresponding to the Gerstenhübel Bed. In ZNO the Wildegg Formation is thinner than in NL and only one interval of Marly Malm is differentiated (**ZNO-MM**, Time interval *154.8_Oxf_975_Top_Dogger_Gr* to *154.8_Oxf_300_nTop_Wildegg_Fm*).

In a next step, the abstracted units were classified regarding their hydrogeological significance based on the data compiled in Chapter 4 (refer to blue and grey arrows in Encl. 2-3a to 2-3c). Deep aquifers were differentiated into regional aquifers (Muschelkalk, Hauptrogenstein and Malm), local aquifers at site scale (ZNO-DSK/Seebi Member, JO-DK/Gansingen Member) and local aquifers confined to channels (SK in all geological siting regions). Zones with potentially increased transmissivity (fractured “hard beds” or local facies variation) were differentiated based on their thickness. Beds/units with 2 – 8 m thickness (e.g. CL/Beggingen Member, SCD, NL-CM/Gerstenhübel Bed) are separated from beds/units >8 m thickness (NLW-/NLE-CD/«Herren-wis Unit»). The threshold of 8 m is based on observations from hydraulic packer tests in the Lias Group, Dogger Group above Opalinus Clay and Malm Group (see Section 5.6.3.2 of Nagra 2024e).

3 3D-horizon models

3.1 Introduction

In this chapter and especially under Encl. 3-1 to 3-10 we provide an overview of 3D surfaces of the abstracted units defined in Chapter 2. The enclosures include a 3D view of the model, selected depth maps and thickness maps.

The model horizons are not intersected with seismically mappable faults of significant throws within the AOI. Structural maps are presented in Section 4.3.4 of Nagra (2024e) as well as in Section 5.3 of Nagra (2024a, 2024b, 2024c).

3.2 Database and method

Input data for the 3D horizons include the results from the deep boreholes and the 3D-seismic data interpretation. The coverage by deep boreholes increased from one deep borehole per siting region to 3 boreholes in JO, 5 in NL and 4 in ZNO. In contrast to SGT Stage 2, 3D-seismic datasets are available for all siting regions.

The interpretation of the 3D-seismic surveys is documented in Nagra (2024a) (JO), Nagra (2024b) (NL) and Nagra (2024c) (ZNO). The interpretation includes full survey time domain interpretation for seismic key horizons of Mesozoic units and fault interpretations. The full-survey interpretations helped to determine the smaller area of interest (AOI; see Encl. 3-1), which includes the potential repository zone. Within the AOI additional horizons were interpreted and a depth conversion of the horizons was carried out. The depth converted horizons served as a base for the site models.

The modelled surfaces use the detailed seismic interpretations and borehole data inside the areas of interest. Time – depth conversion was conducted with layer-based velocity models. They were built in time domain using the AOI seismic horizon interpretation (Nagra 2024d).

As part of the modelling process, the untied depth-converted horizons were well-tied to the associated stratigraphic markers in the boreholes and additional horizons which could not be interpreted in the seismic (see Nagra 2024a, 2024b, 2024c) were added.

Depth converting a time-domain horizon or interpretation with these velocity models preserve the general structure of the geological horizon but will not perfectly fit the drilled well tops. The surfaces thus were adjusted to the well tops. For the horizons also acting as velocity breaks in the velocity models, the adjustment is mostly done within a 1,000-m influence radius around the boreholes, to fit the chronostratigraphic well tops. If untied depth horizons show residuals to the drilled well tops which are not distributed randomly around null, a compensating bulk shift may be applied before performing the radial adjustment to the borehole data. This occurs, for example, when the horizon is not a velocity break but within a section with a vertical velocity trend.

As already mentioned, some of the horizons defined in Chapter 2, have not been interpreted in the seismic dataset and were thus created using over- and/or underlying horizons and well-controlled thickness maps (see Encl. 3-2). Top Opalinus Clay (170.9_Aal_300[1]) in NL for example is not associated with a marked change in acoustic impedance and, consequently, the stratigraphic horizon is in a seismically transparent zone (with multiples; see Nagra 2024b for details). This horizon therefore was created using Base Opalinus Clay (174.7_Toa_100) as a

[1] Here and in the following we use the abbreviated horizon names according to Encl. 2-4a_Stratigraphic Framework.

reference and an isochore map for the Opalinus Clay based on the well data. The isochore map implements a slight increasing thickness trend towards north-northwest and reflects the rather constant thickness measured in the boreholes.

The resulting horizon surfaces were used to calculate isochore maps (true vertical thickness) for selected intervals (see section 3.3).

The depth and thickness uncertainties are discussed in (Nagra 2024d).

3.3 Resulting thickness and depth maps

The layer models include the horizons listed in Encl. 3-2. The enclosures provide a general insight to the models on different aspects, such as depth maps and true vertical thicknesses maps of selected intervals (e.g. host rock, upper and lower confining units). The vertical delineation of the confining units between Opalinus Clay and nearest aquifers is discussed in Section 4.9 of Nagra (2024e), and also indicated in Encl. 3-2a-c.

Encl. 3-3 shows a 3D view of the resulting layer model including the abstracted units defined in Chapter 2. Encl. 3-4 and 3-5 show the depth maps of the host rock in metres above sea level. Encl. 3-6 to 3-10 show the true vertical thickness of the confining units and the host rock.

In the following paragraphs selected individual depth and thickness maps are described in more detail.

Depth map Top and Base Opalinus Clay (Enclosures 3-4a – c & 3-5a – c)

The depth maps show the geometry of the surfaces delimiting the host rock in metres above sea.

Thickness map of the upper confining units (Enclosures 3-6a – c)

According to Chapter 4 of Nagra (2024e) the following horizons were used for thickness calculation. The base of the upper confining units is in all site models Top Opalinus Clay (170.9_Aal_300). In NL & ZNO the top of the upper confining units is the Top Wildegg Formation (154.8_Oxf_300), while in JO it is the Top Passwang Formation (168.2_Baj_100).

In JO, the top of the upper confining unit (i.e. Top Passwang Formation (168.2_Baj_100)) coincides with a level within a geologically heterogenous interval, where facies transitions and interfingering translate into a complex seismic imaging. Therefore, several interpretation attempts have been made, which result in different picking scenarios. As a result, such a horizon has to be considered of very low confidence, which directly affects the certainty for the upper confining units.

In NL the Wildegg Formation thickens to the west. This also imprints to the thickness map of the upper confining units.

The seismic horizon defining the Top Wildegg Formation (154.8_Oxf_300) in ZNO has been interpreted considering the variable seismic quality of this stratigraphic level. The amplitude is very continuous in the western sector of the AOI but becomes discontinuous towards the east. The relatively small thicknesses striking north-south, east of the Benken well are already located in an area with clear and continuous reflections.

Thickness map of the Opalinus Clay (Enclosures 3-7a – c)

The Top Opalinus Clay (170.9_Aal_300) in NL is not associated with a marked change in acoustic impedance and, consequently, the stratigraphic horizon is in a seismically transparent zone (with multiples; see Section 5.2.3 of Nagra 2024b for details). The Top Opalinus Clay (170.9_Aal_300) horizon was therefore created using Base Opalinus Clay (174.7_Toa_100) as a reference and an isochore map of the Opalinus Clay based on the stratigraphic markers at the wells. Due to the low impedance contrast at the Top Opalinus Clay (170.9_Aal_300) this isochoring is a robust solution to map Top Opalinus Clay (170.9_Aal_300).

TRU1 is the borehole with the deepest drilled Opalinus Clay in ZNO and the fastest velocities within the Opalinus Clay in this siting region, which is likely an effect of compaction of these sediments. The velocity model uses a constant velocity for the Opalinus Clay based on the data of the four boreholes. Thus, the thickness in ZNO might slightly be underestimated in the deeper (eastern) part of the siting region outside the area of control of the TRU1 borehole.

Thickness maps of the lower confining units between Base Opalinus Clay and the Keuper aquifer (Enclosures 3-8a – c)

The lower confining units range from Base Opalinus Clay (174.7_Toa_100) to Top Gansingen Member (227_Car_100) in JO, to Top Ergolz Member (227_Car_200) in NL and to Top Seebi Member (208.5_Nor_100) in ZNO (see Encl. 3-2, Nagra 2024e).

As outlined above, challenges of interpreting Base Opalinus Clay (174.7_Toa_100) in NL also affects the thickness maps of the lower confining units.

Total thickness map of confining units and host rock (Enclosures 3-9a – c)

The Enclosures show the total thicknesses of the confining units and host rock.

Potential additional confining units (Enclosure 3-10)

In NL, the Keuper aquifer is occurring only locally related to sandstone channels in the Ergolz Member (see Section 4.5.3.10 of Nagra 2024e for further information). Consequently, the units between to Top Ergolz member (227_Car_200) and Top Muschelkalk Group (237_Lad_400) may additionally contribute to the transport barrier. The thickness of this interval in NL is thus shown in an additional Enclosure 3-10.

4 Mineralogy and petrophysical rock properties

4.1 Introduction

Mineralogy, especially the clay-mineral content, exerts fundamental control on diffusion and sorption properties, and the self-sealing capacity (Chapter 5 of Nagra 2024e). Besides mineralogy, the basic petrophysical rock properties are relevant parameters for a number of geomechanical, geochemical, geophysical and transport properties (see e.g. the following chapters in this report, Nagra 2024e or Glaus et al. 2024).

This chapter documents the data and concepts used to determine recommended parameter ranges and gives a brief overview of the results in the form of tables and overview figures.

4.2 Database

The quantitative mineralogy, porosity and grain density data discussed here stem from multi-mineral analyses (MultiMin). The MultiMin approach is based on the calculation of a theoretical log response from an assumed mineralogical content, porosity and pore water composition and the comparison of the results with actual petrophysical log measurement. Parameters are then adjusted until the error between theoretical and actual logs are minimised. A more detailed description of the MultiMin methodology and results of these analyses for the TBO boreholes (Tab. 1-1) and for the older Benken, Weiach and Riniken boreholes is provided in Becker & Marnat (2024). However, information from the three older boreholes is not of the same quality compared to data from the more recent boreholes due to technical and scientific advances in the last decades. Therefore, especially for the characterisation of the siting regions, data from these older boreholes has been used in a qualitative way (e.g. to define the abstracted geological units, see Chapter 2) but has been excluded from quantitative analyses further described in this chapter.

4.3 Methodology

Continuous data of the MultiMin analyses along each borehole was grouped according to the depth intervals of the abstracted units described in section 2.3 to determine unit-specific values of mineralogy and basic rock properties. The vertical variability of these properties per borehole can be determined using geostatistical methods. Here, basic geostatistical values (medians) for the main mineralogical content (Clay-minerals, Carbonates and quartz + feldspars; see Encl. 4-1a – c) and basic petrophysical rock properties (porosity and density; see Encl. 4-2a – c) for the determined units are reported. Outliers are estimated based on the 5 and 95 percentiles and excluded. The relevant parameters calculated are reported in sheets 4_1 to 4_3 in Encl. 7-1.

The upper and lower boundaries of most units were defined based on lithostratigraphic observations (see Chapter 2). However, “hard beds” in the upper Dogger (SCD) and possible channels in the Keuper (SK) were classified based on conceptual models related to their hydro-geological or mineralogical properties. This classification is described in more detail in the following two sections.

4.3.1 Differentiation of SCAD and SCD units

As emphasised in Section 2.3, several calcareous layers (Sandy-Calcareous Dogger, SCD) occur within the Sandy-Calcareous-Argillaceous Dogger (SCAD). The vertical extent of the SCAD unit in each borehole can be determined based on lithostratigraphic information. To delineate the SCD layers intercalated within the SCAD, a cut-off value at a clay-mineral content of 20 wt.% was

applied (see Fig. 4-1). Using such a cut-off value also allows for thickness determination of the SCD layers on a per borehole basis which was used to estimate the percentage of SCD to the combined SCD and SCAD unit thicknesses (see Fig. 4-2).

The choice for the selection of 20 wt.% as a cut-off value for the clay-mineral content is based on two main points: i) it is consistent with observations from hydraulic packer tests indicating much stronger scatter of hydraulic conductivity in intervals below that cut-off value (Fig. 5-42 of Nagra 2024e), and ii) it is consistent with reduced self-sealing potential of faults for intervals with clay-mineral contents lower than the cut-off value (Section 5.7 and Fig. 5-57 of Nagra 2024e). It is also consistent with cut-off values used previously (Section 4.2 of Nagra 2014b).

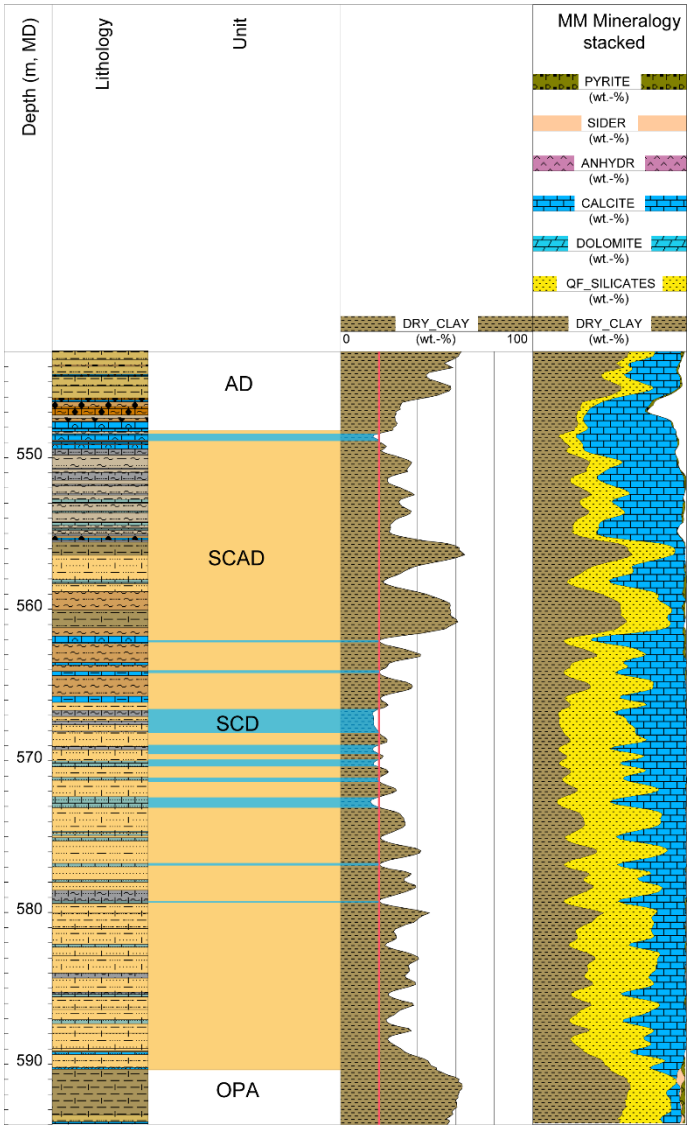

Fig. 4-1: Example of discrimination of SCAD and SCD units in the borehole MAR1

The bluish rectangles in the "Unit" track enclose the areas where the clay-mineral content is <20 wt.% (red line in the DRY_CLAY track which represents the clay-mineral content determined from the MultiMineral interpretation). The MM Mineralogy track displays the interpreted main mineral content (SIDER = Siderite, ANHYDR = Anhydrite, DRY_CLAY = clay-mineral content).

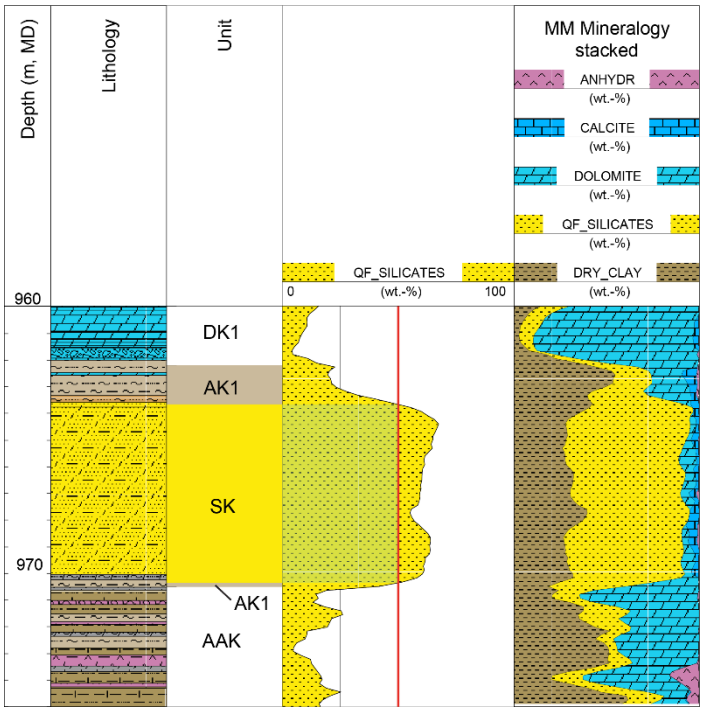

Fig. 4-2: Example of the determination of SK within AK1 in STA2

Values below 50 wt.% QF-silicates are counted to AK1. Values above 50 wt.% (red line in track QF_SILICATES) are counted towards the channels (SK, yellow colors in the "Unit" track). The 50 wt.% cut-off is also indicated by the light green square in the QF_SILICATES track. The MM Mineralogy track displays the interpreted main mineral content (ANHYDR = Anhydrite, DRY_CLAY = clay-mineral content) from the MultiMineral interpretation.

The proportion of SCD in SCAD for the different siting regions is expressed as a percentage of SCD of the combined thickness of SCAD+SCD. In JO, the BOZ2 borehole has only 2 very thin layers which represent just 1% of the total thickness while the BOZ1 borehole has 7 layers of variable thickness representing 18% of the total. ZNO shows comparable values ranging between 9% (in MAR1; see Fig. 4-1) and 20% (in TRU1). In NL, using a strict cut-off value of 20 wt.% on the clay-mineral content, no sandy-calcareous "hard beds" were identified (i.e. the clay-mineral content is always above 20 wt.%). However, two samples in the «Murchisonae-Oolith Formation» just above the Opalinus Clay in the BAC1 borehole yielded low clay-mineral contents of around 10 wt.% only (see Nagra (ed.) 2023a: Table 2-1 in Summary plot). Based on expert judgement, the upper bound of the thickness proportion of SCD in SCAD in NL could be up to ca. 10%.

4.3.2 Differentiation of SK and AK1 units

The same general principle as for the SCAD/SCD was used to determine channels with elevated transmissivities (Sandy Keuper, SK) within the Argillaceous Keuper (AK1). Here, a cut-off value of 50 wt.% for quartz and feldspars (QF) was used (see Fig. 4-2). This cut-off value is based on detailed analyses of hydraulic packer test results notably in the STA2 borehole, in which overlaps of test intervals led to the conclusion that a significant increase in transmissivity is associated with intervals where QF-silicates are the dominant mineral phase. To distinguish possible channels from e.g. over bank deposits, an additional criterion of a minimum thickness (50 cm) was applied to assign intervals to SK units. Due to this minimum thickness criterion, no SK units are identified in the boreholes of JO. But the minimum thickness criterion may be met between boreholes and for this case SK parameter values from NL should be used.

4.4 Results

Sheets 4_1 to 4_3 of Encl. 7-1 give an overview of the data for each borehole and combined per siting region. The general nomenclature for units introduced in Chapter 2 is used. As a reminder, not all units occur in each borehole of a single siting region. One example is the «Herrenwis Unit» (E-CD and W-CD), present in the NL siting region only.

4.4.1 Mineralogy

The main mineralogy of clay, carbonates (calcite and dolomite) and silicates (quartz and feldspars) are given in the form of boxplots in Encl. 4-1a – c and in the form of tables (5, 50 and 95 percentiles) for total clay content in Encl. 7-1, sheet 4_1. Other mineralogical content, such as salt, anhydrite or minor minerals like pyrite, are not shown here because they generally are rarely used to determine geomechanical, geochemical or transport properties. In host rock and confining units, the percentage share of these units is generally low. However, in the units below (Bänkerjoch-Fm and Muschelkalk Group) a high anhydrite and/or salt content has been interpreted/observed in some boreholes. Hence, boxplot means in enclosure 4-1 do not necessarily add up to 100% which is especially obvious e.g. in the ANK, AAK and MAK units which show considerable amounts of anhydrite. Continuous profiles of mineralogy for all TBO boreholes, including salt and anhydrite, are given in the enclosures of Becker & Marnat (2024).

4.4.2 Basic petrophysical rock properties (grain density, porosity)

The percentiles (P5, P50 and P95) for both porosity and grain density are given in Encl. 7-1 in sheets 4_2 (porosity) and 4_3 (grain density) together with overview plots in Encl. 4-2a – c.

5 Hydrogeological properties and conditions

5.1 Introduction

Characterised by very low hydraulic conductivities, the Opalinus Clay and its confining units form excellent aquitards in which transport at the formation scale is diffusion dominated. Their hydraulic barrier effect is also supported by hydrogeochemical investigations and observed trends indicating anomalous pore pressures in long-term monitoring system (Chapter 5.6.5 of Nagra 2024e). It is responsible for the hydraulic decoupling between the over- and underlying aquifers of the Malm, Hauptrogenstein, Keuper and Muschelkalk.

Advective dispersive transport dominates in these aquifers where groundwater flow is driven by topography-controlled lateral hydraulic gradients and comparatively high hydraulic conductivities. Acting as a hydraulic boundary condition of the aquitard systems, the aquifers exert a strong control over the hydraulic heads in the host rock and confining units.

The hydraulic heads (or pore water pressures) in the Opalinus Clay are relevant for the design of the deep geological repository, notably with respect to effective stresses.

5.2 Database

The primary datasets to derive recommended parameter bandwidth of the rock mass hydraulic conductivities (Sections 5.3.1 and 5.3.2) are (Tab. 5-1):

- Estimated hydraulic transmissivities and derived hydraulic conductivities from in-situ hydraulic packer tests performed in the host rock, confining units, and aquifers in the siting regions. The metric to decametric test intervals can cover different lithologies and variable degrees of tectonic overprint.
- Matrix hydraulic conductivities parallel and perpendicular to bedding from laboratory experiments conducted on centimetric to decametric drill-core samples. The testing program mainly focused on the Opalinus Clay, and on the Dogger above the Opalinus Clay and Lias units to a lesser extent. This dataset consists of several test types (Tab. 5-1) conducted under different conditions.

The mineralogy and porosity of the rock, along with the structural inventory (tectonic overprint) in the intervals of the hydraulic packer tests, were also considered to investigate possible relationships with the rock hydraulic conductivities.

The following complementary datasets were used conceptually as independent evidence of low hydraulic conductivities in the aquitards (Tab. 5-1):

- Porewater and groundwater hydrogeochemical investigations
- Hydraulic head measurements from long-term monitoring systems

The parameter bandwidth for hydraulic heads and gradients (Sections 5.3.4 and 5.3.5) are primarily based on the long-term monitoring systems (LTM) measurements of the Benken borehole and the newly equipped BOZ1, STA3 and MAR1 boreholes. Hydraulic heads derived from hydraulic packer test analysis were also considered for the aquifers (Tab. 5-1). Note that the LTM of the Benken borehole is particularly relevant as the measurements in the aquitards could take decades to recover from drilling activities. Simulation results of the groundwater flow models were mainly used as complementary data.

Tab. 5-1: List of hydrogeological parameters

The Dossier numbers refer to the TBO reports listed in Tab. 1-1.

Property	Primary data	Complementary data
Hydraulic conductivities and transmissivities	In-situ hydraulic packer tests and fluid logging (TBO Dossier VII, Beauheim 2013) Laboratory tests: oedometric and constant head tests (TBO Dossier IX), and advective displacement (TBO Dossier VIII)	Structural inventory (TBO Dossier V) MultiMin data (TBO Dossier X), Porewater hydrogeochemistry and hydraulic heads from long-term monitoring (TBO Dossier VIII, Nagra 2024e, e.g. Longridge et al. 2024)
Hydraulic heads and hydraulic gradients	Long term monitoring system (e.g. Longridge et al. 2024) and in-situ hydraulic packer tests and fluid logging (TBO Dossier VII)	Groundwater flow models (Nagra 2024f, Gmünder et al. 2014)

5.3 Conceptual considerations to derive parameters

Section 5.3.1 provides the rationale for the derivation of the recommended equivalent hydraulic conductivities for the rock mass (i.e. the rock matrix and additional tectonic overprint) as considered representative in the area of the deep geological repository. The provided values are mainly based on the results and conclusions of the Nagra's deep borehole investigations (TBO Dossiers listed in Tab. 1-1, Nagra 2024e).

In Section 5.3.2, transmissivities for faults are formulated based on available data, concepts and analogues. These values aim to cover potentially unobserved faults with enhanced transmissivities to test the robustness of the system regarding transport (performance assessment).

The rationale for the derivation of the lateral hydraulic gradients in aquifers, and hydraulic heads and vertical gradients respectively in and across the Opalinus Clay is provided in the subsequent Sections 5.3.3 and 5.3.4 respectively.

5.3.1 Hydraulic conductivities of the rock mass parallel to bedding

5.3.1.1 Representativity of the datasets

The hydraulic packer tests covered intervals of meters to decameters in length, which is the scale of interest for the deep geological repository, e.g. covering the size of future tunnels and cumulated with several tests also a significant part of the formation thickness. Furthermore, the test intervals cover both intact and fractured or faulted rock intervals, and the derived hydraulic conductivities reflect the ones of the rock masses. The hydraulic packer test results therefore do not need any scaling and are considered the key data to derive recommended bandwidths of hydraulic conductivities for the rock mass.

In the Dogger and Lias sections, the hydraulic packer test interval lengths covered approximately 40 to 70% of the total drilled thickness and generally included intervals with tectonic overprint. Hence, they provide excellent coverage of the units. The packer test results are therefore considered to provide a representative estimation of the formation hydraulic properties in the direction parallel to bedding. In the confining units, the tests generally cover various (sub)units

that can display contrasting hydraulic conductivities. The presence of slightly conductive fractures (e.g. in clay-poor layers) and/or facies (e.g. quartz and feldspar-rich beds) can dominate the test results, taking over on the hydraulic signature of the remaining low permeability units. In such a case, a workflow was applied to isolate the hydraulic properties of each (sub)unit covered by the hydraulic packer tests (see example for the SCAD & SCD subunits in Section 5.3.1.2).

In the aquifers, testing efforts were concentrated on the most permeable zones of the formations identified by fluid logging (in the Malm), mud losses, and/or structures detected on core and/or image logs. This approach gives a representative estimation of the formation transmissivities.

Assessing the representativity of the datasets laterally is more challenging, especially in low-permeability units such as Opalinus Clay where the radius of investigation of the hydraulic packer tests is limited to <1 m behind the borehole wall (de Marsily 1986). But the following observations provide confidence that the measurements can indeed be considered representative also spatially (Nagra 2024e): i) small variability of the packer test results between the boreholes, ii) good lateral correlation of the sedimentary sub-facies (mineralogy and porosity), iii) small variation of hydraulic conductivities in sub-facies as constrained on laboratory measurements, iv) independent evidence from porewater investigations and long-term monitoring systems, which are consistent with the very low intrinsic hydraulic conductivities of these formations.

For the Opalinus Clay, a comprehensive laboratory testing programme was done to constrain matrix conductivities of the intact rock. The tests covered the observed spectrum of porosity and mineralogy of the formation as well as the effective stress range at in-situ conditions. The range of measurements is therefore considered representative at the scale of measurement (i.e. centimetre to decimetre). Given the larger lithologic variability, this is only partly the case for the other units.

5.3.1.2 Derivation of recommended lateral hydraulic conductivities

The applied methodology to derive recommended parameter bandwidth of hydraulic conductivities for units defined in Section 2.3 is explained in the following for the OPA unit, and the SCAD & SCD subunits.

OPA unit (Opalinus Clay)

The hydraulic conductivities in OPA are low and vary within a narrow range (approximately 1×10^{-14} and 1×10^{-13} m/s), within the spectrum of matrix hydraulic conductivities (approximately 1×10^{-15} to 1×10^{-12} m/s) as shown in grey on Fig. 5-1a and Fig. 5-1b. This highlights both the relative homogeneity of facies and the absence of a relevant impact of the tectonic overprint on its hydraulic conductivities. The median of the hydraulic conductivities from the hydraulic packer tests is 4×10^{-14} m/s (Fig. 5-1b). The wider distribution of matrix hydraulic conductivity from laboratory tests in comparison to the one of the hydraulic packer tests can be explained by:

- The scale of measurement: hydraulic conductivities of small-scale samples are affected by local lithological variations while these effects are averaged in the case of the hydraulic packer tests.
- The heterogeneity of the laboratory dataset: the different test types were performed under different conditions (different testing apparatus, confining pressure etc.).

The estimated transmissivity of the interval T_{TEST} is expressed as the product of the hydraulic conductivity K and the length of the test interval L:

$$T_{TEST} = K \times L \qquad \textit{Eq. 5.1}$$

As a result of the small variability of the hydraulic conductivities in the Opalinus Clay, a linear relationship exists between T and L (Fig. 5-1c). Taking advantage of this, an average hydraulic conductivity $\widehat{K}_{OPA}$ for the dataset can be calculated by the mean of a linear regression of the form (Fig. 5-1c):

$$\hat{T} = \widehat{K}_{OPA} \times L \qquad \textit{Eq. 5.2}$$

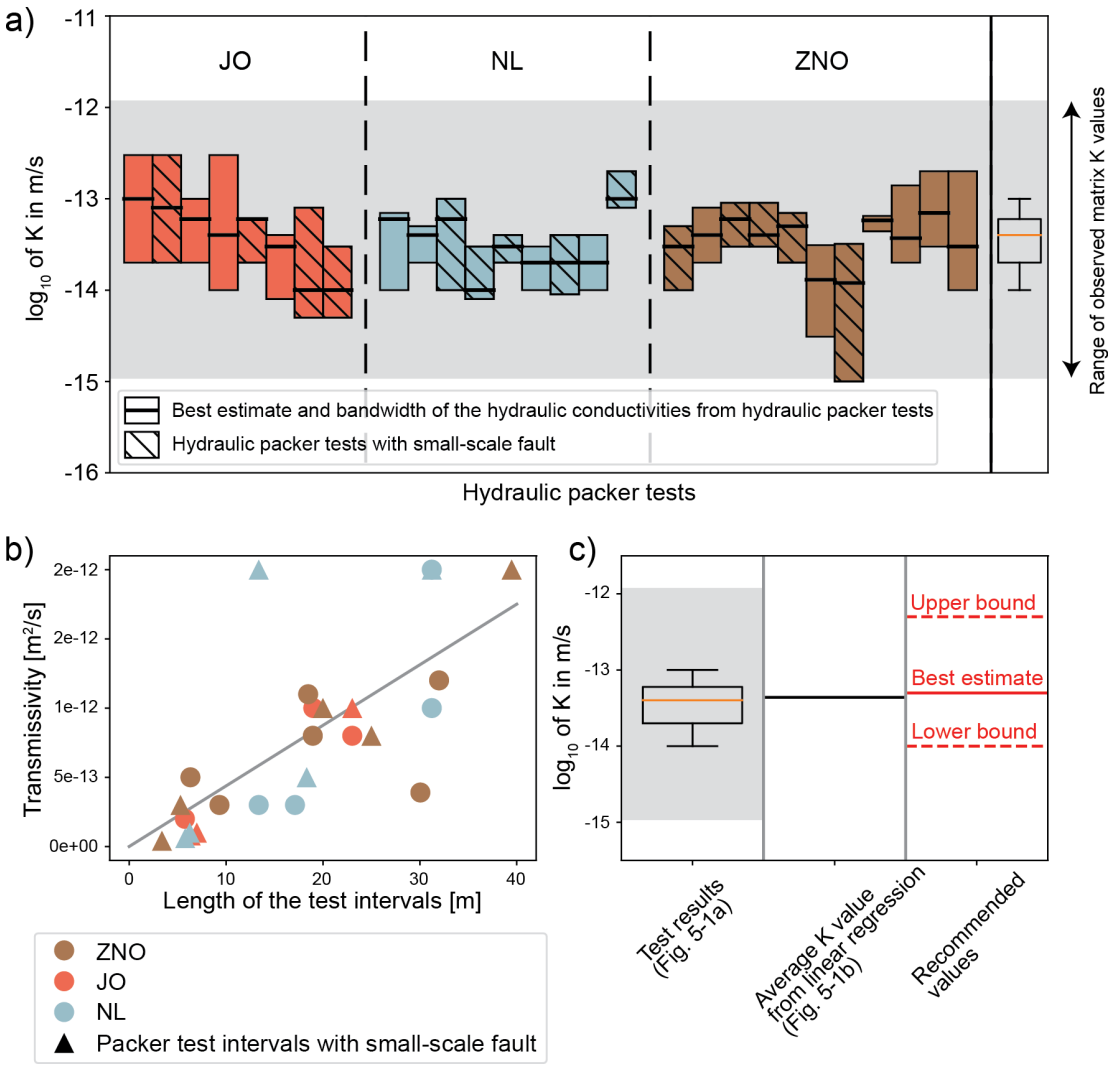

Fig. 5-1: Interpretation of the hydraulic dataset from the Opalinus Clay

a) Results of the in-situ hydraulic packer tests, grouped by siting region. The bar chart shows the best estimate and the bandwidth of the derived hydraulic conductivities. The range of observed matrix properties (from laboratory tests) is displayed in grey. The box plot on the right displays the best estimates of the hydraulic conductivities derived from hydraulic packer tests. b) Cross plot of the transmissivities as a function of the length of the test intervals in the Opalinus Clay. The displayed dataset includes the results of the TBO boreholes and BEN (Nagra 2024e). c) Summary figure showing the box plot of sub-figure (a) in comparison with the average hydraulic conductivity derived using linear regression in (b) and recommended values (best estimate, upper and lower bounds) for the rock mass of the Opalinus Clay.

An average hydraulic conductivity of 4.4×10^{-14} m/s, representing the slope of the regression line (Fig. 5-1c), is inferred. The low associated p-values (<0.01) suggest that the latter value is statistically significant.

Based on these results, the best estimate of the expected hydraulic conductivity is set to 5×10^{-14} m/s (Fig. 5-1d).

While the lower bound of hydraulic conductivity is set to 1×10^{-14} m/s, the bandwidths of a few hydraulic packer tests extend further lower. In comparison, values below 1×10^{-14} m/s are rare in the drill-core sample dataset and are unlikely when equivalent hydraulic properties are inferred to the metric to decametric scale using laboratory measurements. The lower bound was thus set to 1×10^{-14} m/s (Fig. 5-1d).

The upper bound was fixed to 5×10^{-13} m/s (Fig. 5-1d) to fully cover the range of hydraulic conductivities measured from the hydraulic packer tests and inferred equivalent hydraulic conductivities at the metric to decametric scale (i.e. the scale of the hydraulic packer tests) using matrix hydraulic conductivities from drill-core samples. For comparison purpose, a hydraulic conductivity of 4×10^{-13} m/s was derived for a 30 m test interval at the base of the Opalinus Clay of the Schafisheim borehole, which includes an approximately 20 m thick zone of strongly deformed Opalinus Clay (not observed in the siting regions).

SCAD & SCD units (Passwang Formation, «Murchisonae-Oolith Formation» to «Humphriesioolith Formation»)

As emphasised in Sections 2.3 and 4.3.1, the Sandy-Calcareous-Argillaceous Dogger (SCAD) is intercalated with the Sandy-Calcareous Dogger (SCD). A cut-off clay-mineral content value of 20 wt.% was used to discriminate the SCD layers.

The hydraulic conductivities measured in the stack of the SCAD & SCD units are generally low (Fig. 5-2a and Fig. 5-2b) but vary within a larger spectrum compared to the Opalinus Clay (2×10^{-14} and 2×10^{-12} m/s, median of 2×10^{-13} m/s; Fig. 5-2a). The highest values fall outside of the range of matrix hydraulic conductivities (Fig. 5-2a and Fig. 5-2b) derived from the limited dataset.

While in the Opalinus Clay the test interval length is generally constrained within the bounds of the formation, test intervals performed in the SCAD & SCD units generally cover both subunits (Encl. 5-1a, 5-1b and 5-1c), and sometimes overlap with adjacent units. The challenge thus relies in the isolation of the hydraulic conductivities of the subunits.

A representative range of hydraulic properties was derived for each packer test, following steps 1 and 2 described hereafter.

1) First estimate of range of K_{SCAD} and K_{SCD}

As a first step, the range of hydraulic conductivities derived from the test intervals with clay content >20 wt.%, that is without any SCD layers (according to the 20 wt.% cut off), was assumed representative for the SCAD unit. This range of value was then used to estimate a range of hydraulic conductivities for the clay-poor layers of the SCD units (Fig. 5-2b) assuming that:

$$T_{Test} = K_{SCAD} d_{SCAD} + K_{SCD} d_{SCD} \qquad \textit{Eq. 5.3}$$

Where T_{Test} is the test interval transmissivity, K_i is the hydraulic conductivity of unit i, and d_i is the thickness of unit i accommodated within the test interval.

2) Refined range of $\boldsymbol{K_{SCAD}}$ and $\boldsymbol{K_{SCD}}$

Hydraulic packer test results do indicate an E-W trend (JO to ZNO siting region) with increasing hydraulic conductivity values (Fig. 5-2a). The above considerations, with different bounds for K_{SCAD} and K_{SCD} were therefore complemented with a refined analysis on the influence of mineralogy and porosity. A negative correlation was found between the carbonate content in the test intervals (median of the carbonates content constrained from MultiMin, Fig. 5-2c) and the hydraulic conductivities from the hydraulic packer tests.

Taking advantage of this correlation, and considering a layer system composed of layers A and B, a linear system of equation of the following form was built:

$$d \cdot K = T = \begin{pmatrix} d_{A1} & d_{B1} \\ d_{A2} & d_{B2} \\ \vdots & \vdots \\ d_{AN} & d_{BN} \end{pmatrix} \cdot \begin{pmatrix} K_A \\ K_B \end{pmatrix} = \begin{pmatrix} T_1 \\ T_2 \\ \vdots \\ T_N \end{pmatrix} \qquad \textit{Eq. 5.5}$$

Where the subscripts A and B refer to layers based on a cut-off value of carbonate content to be defined, K_A and K_B are the hydraulic conductivities of layers A and B, while d_{Ai} and d_{Bi} are the total thickness of the layers A and B in the test interval i.

Solving this inhomogeneous linear system of equation for K_A and K_B sequentially using different cut-off values of carbonates content leads to a best cut-off of 22 wt.% (Fig. 5-2d), characterised by the lowest associated error (i.e. means squared error between simulated and observed transmissivities).

Two average hydraulic conductivities (i.e. one for the layer A with a carbonates content <22 wt.% and one for the layer B with a carbonates content ≥ 22%) are derived along each borehole. The equivalent K_{SCAD} and K_{SCD} are then calculated from the distribution of SCAD and SCD layers (Fig. 5-2e).

The two approaches outlined above are then used in combination to specify bounds for K_{SCAD} and K_{SCD} (Fig. 5-2f). This analysis underlines that:

- The SCD layers show the widest range of hydraulic conductivities, that is between 1×10^{-14} and 5×10^{-11} m/s. While low hydraulic conductivities are typical for the carbonate-rich "hard beds", the highest values are expected in quartz and feldspar-rich layers. The lowest hydraulic conductivities reflect the average hydraulic conductivities encountered in the carbonate-rich SCD layers.
- The SCAD layers display an intermediate range of hydraulic conductivities between 1×10^{-14} and 5×10^{-13} m/s. The lowest hydraulic conductivities reflect the average hydraulic conductivities encountered in the carbonate-rich SCAD layers.

The recommended hydraulic conductivities of the SCAD unit were set as follows (Fig. 5-2g):

- A best estimate of 1×10^{-13} m/s is set based on the refined statistical analysis described above in the text as well as on the results obtained for other clay-rich units.
- The upper bound is set to 1×10^{-12} m/s based on the highest average hydraulic conductivity derived from the refined statistical analysis described above.
- The lower bound is set to 1×10^{-14} m/s in analogy to the well-constrained dataset of the Opalinus Clay.

The recommended hydraulic conductivities for the SCD unit are defined based on the following considerations (Fig. 5-2g):

- The best estimate was set to the low value of 5×10^{-14} m/s based on the results of the refined statistical analysis. It reflects the dominance of carbonate-rich "hard beds" in the SCD unit in the deep boreholes based on the MultiMin dataset.
- The brittle behaviour of the SCD unit "hard beds" is likely to enhance their bulk hydraulic conductivities. The presence of hypothetical fracture networks was thus accounted for in the definition of the upper bound. To do this, the SCD dataset was extended to include hydraulic packer test results acquired in fractured sections of the analogue CL unit (i.e. thin limestone bed of the Lias). The upper bound (5×10^{-10} m/s) was constrained according to the highest transmissivity measured in association with a subvertical joint in the CL unit of the BAC1 borehole.
- The lower bound (1×10^{-14} m/s) reflects low hydraulic properties of the intact rock, which is the same as for Opalinus Clay.

Remaining units

The table in Encl. 5-2 provides a short description of the methodology adopted for the derivation of the best estimate, upper bound and lower bound of the hydraulic conductivities of the remaining units. Some general observations are provided below:

- The amount of data tends to decrease away from the Opalinus Clay (Encl. 5-1a to 5-1c) reflecting their relevance as a geological barrier.
- The bandwidths of the recommended rock mass hydraulic conductivities tend to increase away from the Opalinus Clay in order to reflect (1) the uncertainty carried out by the amount of available data per unit, and (2) the scatter of hydraulic conductivities due to the general decreasing clay-mineral contents (Nagra 2024e).
- The parametrisation of units with limited datasets mainly relies on the datasets and recommended parameters of analogue units (with similar basic properties).

Additional comments for selected units are provided in Encl. 5-2.

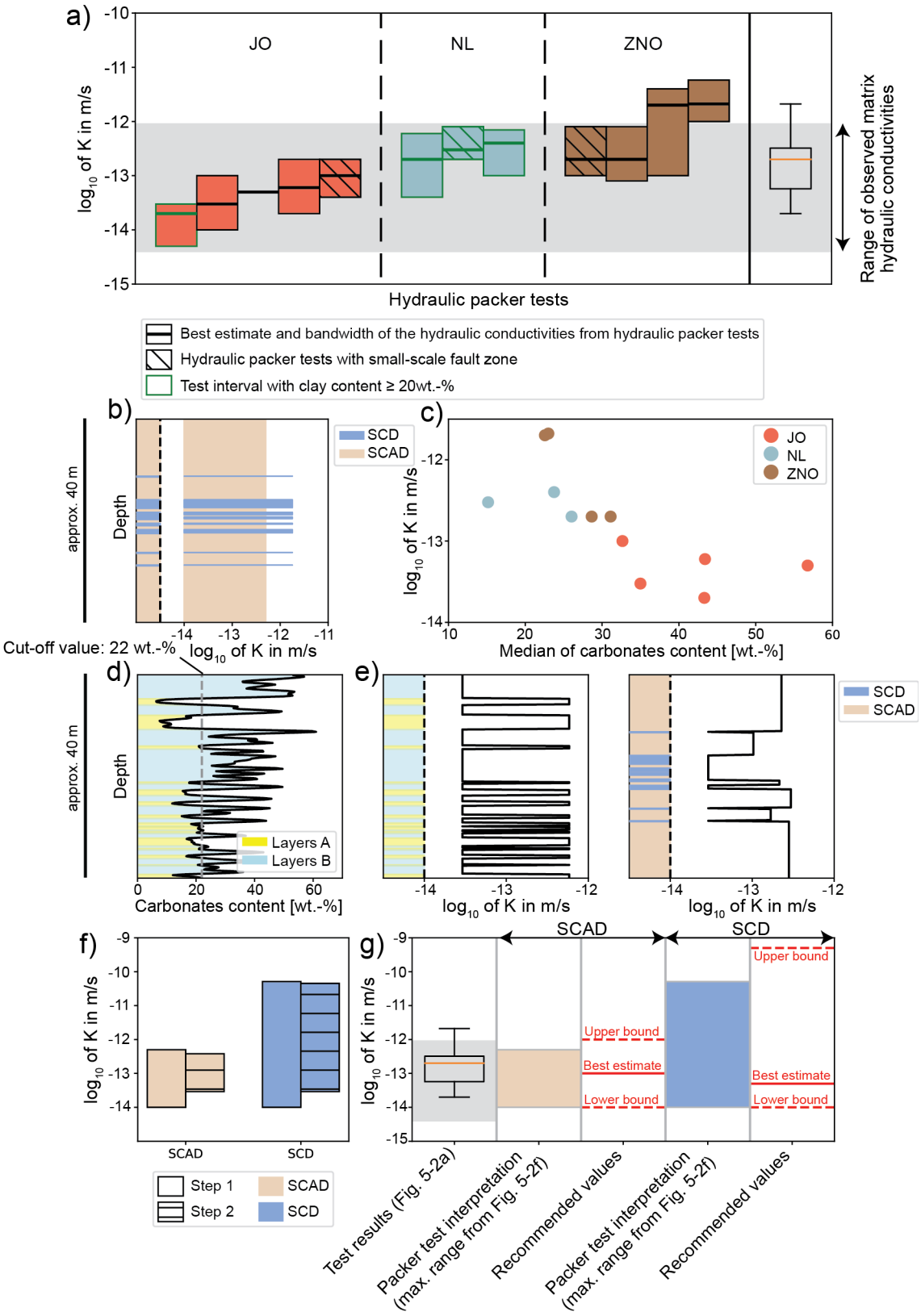

Fig. 5-2: For figure caption see opposite side

Fig. 5-2: Interpretation of the SCAD & SCD hydraulic dataset

(a) Results of the hydraulic packer tests, grouped by siting region. The range of observed matrix hydraulic conductivities properties (from laboratory tests) is displayed in grey. (analogous to Fig. 5-1a) (b) Estimated K_{SCAD} and K_{SCD} (step 1; example test MAR1-BDO1) (c) Negative correlation of hydraulic conductivities with median carbonate content of the test intervals. (d) Profile of carbonate content and cut-off value (22 wt.%) to distinguish layers A and B (example: test interval MAR1-BDO1). (e) Derived hydraulic conductivities for the layers A and B (on the left) and for the SCAD and SCD layers (on the right). (f) Derived ranges of formation hydraulic conductivities of the SCAD and SCD from the hydraulic packer test analysis (steps 1 and 2 in the text). (g) Summary figure showing the box plot of sub-figure (a) in comparison with the maximal range of hydraulic conductivities derived from the hydraulic packer test analysis (steps 1 and 2 in the text) (c) and recommended values (best estimate, upper and lower bounds) for the rock mass of SCAD and SCD subunits.

5.3.2 Anisotropy coefficient

Overall, drill-core samples from the Opalinus Clay tested parallel and perpendicular to bedding do not show any visible systematic anisotropy of their hydraulic conductivities (Fig. 5-3).

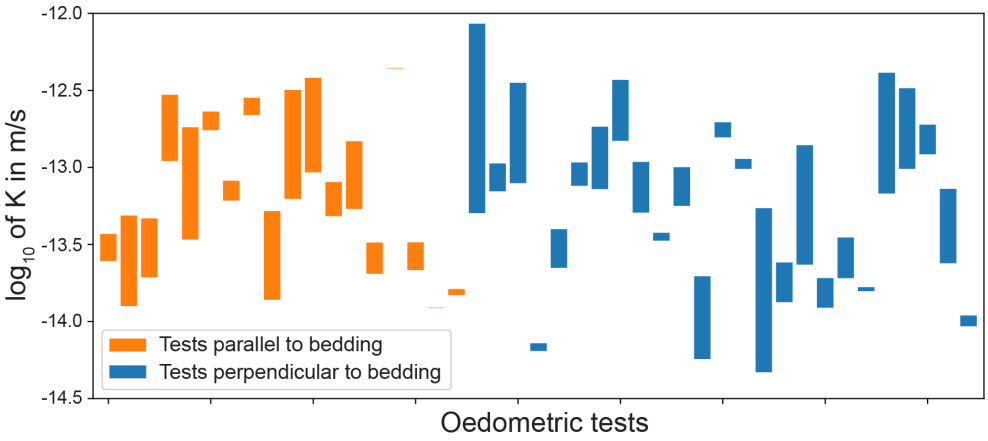

Fig. 5-3: Hydraulic conductivities of Opalinus Clay constrained by oedometric tests

The plot shows the range of hydraulic conductivities for each individual tests. Applied effective stress ranges from 2 to 20 MPa.

The Opalinus Clay displays a layering whether at the formation scale (i.e. the different subunits) or at the macroscopic scale (i.e. bedding). It follows that the variability of its hydraulic properties is expected to be more pronounced perpendicular to the bedding than parallel to it. This results in an anisotropy of its hydraulic properties with the maximal hydraulic conductivity being parallel to the bedding.

This was quantitatively investigated using a synthetic layered model such as the one illustrated on Fig. 5-4.

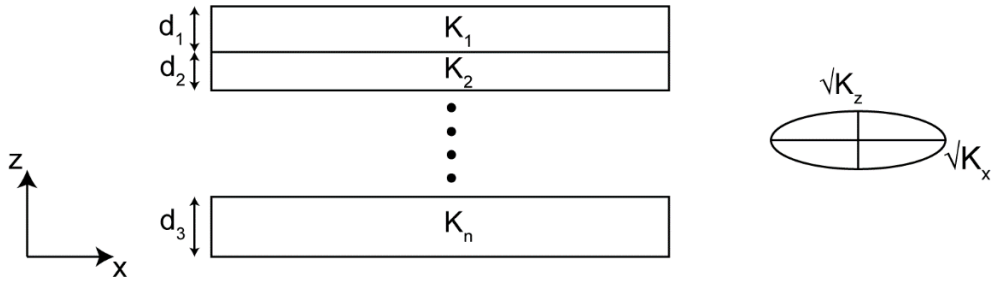

Fig. 5-4: Large-scale anisotropy of a layered geological system consisting of isotropic layers with different hydraulic conductivities (conceptual sketch)

In such a simplified layered system, the equivalent hydraulic conductivities parallel and perpendicular to bedding are respectively quantified in terms of the arithmetic and harmonic means (weighted with the thicknesses of the layers) of the hydraulic conductivities (e.g. Freeze & Cherry 1979 Freeze & Cherry 1979). Here, such a large-scale anisotropy is quantified using *Eq. 5.6*:

$$a_K = \frac{K_x}{K_z} = \frac{1}{d^2}\sum_{i=1}^{n} K_i d_i \sum_{i=1}^{n} \frac{d_i}{K_i} \qquad \textit{Eq. 5.6}$$

Randomly populating the layered model with hydraulic conductivities sampled from matrix hydraulic conductivity distributions (i.e. from drill-core samples) resulted in a best estimate of the anisotropy coefficient of 5 and an upper bound of 10 for the Opalinus Clay. The same exercise repeated using the hydraulic conductivities of the hydraulic packer tests, resulted in an anisotropy coefficient lower than 5. The lower bound was set to 1 and reflects isotropic conditions.

The derived values are considered valid from the tunnel scale to the total thickness of the Opalinus Clay.

The above-mentioned best estimate and bandwidth were further considered for the other clay-mineral-rich units (i.e. SCAD, AL, NL-ARD, AD, AK1 to AK3, JO-AK2/3).

Due to their strong vertical heterogeneity, an anisotropy coefficient ranging from 1 to 10 is recommended for the MM, MM1 and MM2 units, consistent with previous values (Appendix A6 of Nagra (2010) and Section 4.7.3.2 of Nagra (2014b)). No evidence regarding anisotropy was found for the remaining units. They were thus considered as isotropic.

5.3.3 Transmissivities of faults

The intervals targeted as part of the hydraulic packer test program typically include zones with tectonic overprint along the boreholes. The faults covered in the in-situ tests typically range from micro faults to small-scale faults in scale. Given the strong heterogeneity of fault architecture in clay-limestone successions (e.g. Childs et al. 2009, Nagra 2024e), bracketing fault transmissivities cannot only rely on field measurements but should be complemented by concepts and analogues.

Fault transmissivities were thus derived in addition to rock mass hydraulic conductivities (Section 5.3.1) to cover hypothetical and unobserved faults with enhanced hydraulic transmissivities. These values aim to be used to evaluate the deviations from the observations to test the robustness of the barrier system regarding transport in the stack of units (performance assessment).

In Encl. 5-1 a reference value and an upper bound of the expected transmissivities are provided per unit. A lower bound is not provided as hydraulic properties of faults with low or moderate transmissivities are covered in the recommended rock mass hydraulic conductivities (Section 5.3.1). A comparison between transmissivities from the hydraulic packer tests and the best estimate and upper bound of fault transmissivities is provided in Fig. 5-5 to guide through the conceptual approaches applied below.

Based on the experience gained in deep boreholes in the siting regions, the importance of the tectonic overprint on the rock hydraulic conductivities increases with a decreasing clay content (Nagra 2024e). This can be explained by more robust self-sealing of faults but also lower fault rock matrix conductivity (e.g. for siliciclastic rocks: Jolley et al. 2007) with elevated clay-mineral content. But transmissivities of thin clay-mineral poor intervals seem to be less affected by the tectonic overprint compared to the massive carbonate-rich formations.

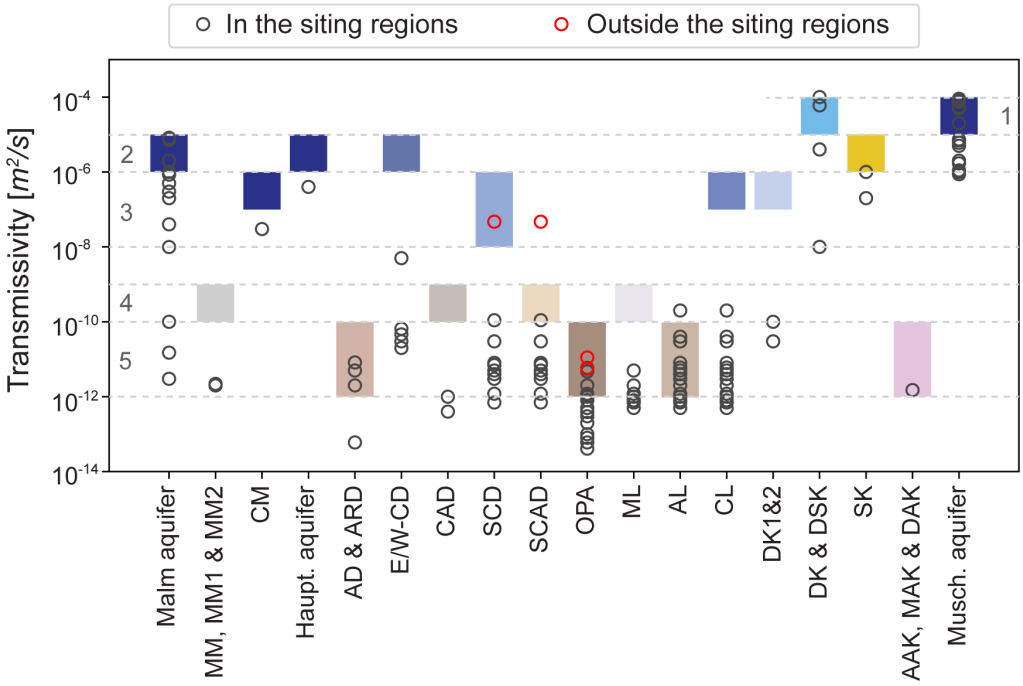

Fig. 5-5: Comparison of unit-specific transmissivities derived from hydraulic packer tests and recommended values for faults

Grey circles represent packer test data acquired in the TBO boreholes, and additionally from the older boreholes BEN, WEI and RIN. Red circles show data from the Schafisheim (OPA unit) and Schlattingen (SCAD & SCD units) boreholes outside the siting regions. For the SCAD & SCD and AL & CL units, the same respective hydraulic packer test dataset is plotted (packer tests cover both units). Coloured boxes represent recommended bandwidth for the reference value and upper bound fault transmissivities in the respective units. The horizontal lines highlight the different categories of units resulting from the application of criteria 1 and 2 (refer to the text below). 1: Dolostone units (thickness >8m), 2: Limestone units (thickness >8 m; include the SK unit), 3: “hard bed” units (thickness <8 m), 4: marly units (including the SCAD unit), 5: clay-rich and anhydrite-rich units.

While fault bulk hydraulic properties depend on a wide variety of parameters and processes (e.g. Fisher & Knipe 1998, Fisher et al. 2018) a simple and conservative approach was adopted to bracket fault transmissivities. The following criteria were applied:

1. **Clay-mineral content:** Three groups: (1) smaller than 20 wt.%, (2) between 20 and 40 wt.%, and (3) greater than 40 wt.%. Groups (1) and (2): further subdivision by lithology were selectively considered (Nagra 2024e).
2. **Geometry:** in the Mesozoic stack, clay-mineral poor units occur as massive carbonate-rich units, but also as thin "hard beds". Based on packer test results, thin "hard beds" are less prone to enhanced transmissivities than the massive formation leading to less deformation (Nagra 2024e).

Following criteria 1, fault transmissivities were firstly derived for the two endmembers, i.e. units with clay-mineral contents <20 wt.% and units with >40 wt.%. Intermediate transmissivities were then assumed for the units with moderate clay contents.

Faults in rocks with clay-mineral contents <20 wt.%

Massive brittle formations of the Malm, Hauptrogenstein and Muschelkalk can exhibit overall high transmissivities in fractured intervals (>10^{-5} m^2/s; Fig. 4-86 of Nagra 2024e). Observed values tend to be even higher in the dolomitic aquifers (up to 1×10^{-4} m^2/s), likely due to a combination of tectonic overprint and the generation of macro-porosity due to dolomitisation. Faults in limestones typically contain a damage zone and a fault core that may become cemented, dolomitised or even karstified. They can act as a barrier to flow across the fault but as a conduit along the fault (Bauer et al. 2016). In comparison, fault in dolostones can typically display wide pulverised damage zones and act as a conduit.

Pesendorfer & Loew (2010) present the detailed analysis of hydraulic packer tests performed in a fractured and karstified limestones in the Lötschberg Base Tunnel (Switzerland). Measured transmissivities range from approximately 10^{-6} to10^{-4} m^2/s, the highest values being observed in karstified intervals. For comparison, transmissive intervals in the Malm aquifers of the NL and ZNO siting regions range from 10^{-7} to 10^{-5} m^2/s.

In the siting regions, karst voids in the Malm aquifer in ZNO and NL are filled with low-permeability sediments, and in JO no karst features were observed in the Hauptrogenstein aquifer. Therefore, the reference value and upper bound of the fault transmissivities in those units were set to 1×10^{-6} and 1×10^{-5} m^2/s. The same transmissivities were assigned to the faults of the unit E/W-CD («Herrenwis Unit») as it consists of a thick clay-poor unit (approximately 40 m in the STA3 and BUL1 boreholes). Note that these values are not reflected in the hydraulic packer test results, which shows transmissivities <10^{-10} m^2/s (and in exceptional cases <10^{-8} m^2/s; see Dossiers VII of reports listed in Tab. 1-1).

Higher values (i.e. one order of magnitude) were considered for the dolomitic units of the Muschelkalk aquifer, and Keuper aquifer in the case of JO and ZNO (i.e. JO-DK and ZNO-DSK).

Lower transmissivities (i.e. one order of magnitude lower than the Malm aquifer unit) were considered for the thinner hard bed units but regionally present CM-Gerstenhübel Bed (NL siting region), CL, NL-DK1 and NL-DK2 following the criteria 2. While the considered values are higher than the ones of the hydraulic packer tests (Fig. 5-5), faulted carbonate-rich "hard beds" can display enhanced transmissivities as supported by the hydraulic packer test results in the Gerstenhübel Bed (Wildegg Formation) in the Olten area (Nagra 2014b) and interpreted mud-losses in the Lias of the Siblingen borehole (Nagra 1992).

The “hard beds” of the SCD unit, which are laterally more variable (Section 4.2.7.2 of Nagra 2024e) were assigned lower transmissivities (i.e. one order of magnitude) than their Lias and Keuper counterparts. Note that the transmissivities of the “hard beds” (SCD) described above are higher than the transmissivity of the hydraulic packer test performed in the Wedelsandstein Formation of the Schlattingen borehole (1×10^{-9} m^2/s) (Fig. 5-5).

Faults in rocks with clay-mineral contents >40 wt.%

In OPA and over-/underlying clay-mineral-rich units (e.g. CAD, AL), the high self-sealing potential and stronger segmentation of faulting hinders strong enhancement of fault transmissivity (Nagra 2024e).

The reference fault transmissivity of the Opalinus Clay (1×10^{-12} m^2/s) reflects typical values from packer tests assuming that one single fault controls the transmissivity per test interval (Fig. 5-40 of Nagra 2024e). The upper bound (1×10^{-10} m^2/s) is based on test results from the Schafisheim borehole and the Mont Terri underground laboratory, and conceptually from comparison with fault gouge analogues (a detailed discussion on fault transmissivity and self-sealing in the Opalinus Clay is provided in Chapter 5 of Nagra (2024e):

- The Schafisheim borehole and Mont Terri underground laboratory are both located in much more strongly deformed areas than the location of boreholes in the siting regions. The packer tests in the Schafisheim borehole yielded the highest transmissivity (1×10^{-11} m^2/s) ever measured in the Opalinus Clay in boreholes at greater depth in Northern Switzerland. The test interval covered an approximately 15 m thick, strongly tectonised interval in the Opalinus Clay south of the Jura Main Thrust. No such faults are observed in the siting regions (Nagra 2023a, 2023b, 2023c).
- Fault slip experiments on the Main Fault at Mont Terri have yielded transmissivities of approximately 1×10^{-10} to 1×10^{-9} m^2/s in the recovery period (several months after stimulation), with a trend to further reduction. Effective stress in the siting regions is higher than at the Main Fault (2024j), and this enhances self-sealing and reduction of transmissivity (Section 5.7 of Nagra (2024e)).
- Generation of fault gouge or swelling in the vicinity of faults can locally enhance porosity compared to the undisturbed rock. But experiments with crushed and re-compressed (remoulded) Opalinus Clay indicate equivalent transmissivities $<1 \times 10^{-11}$ m^2/s even for a 1-m thick gouge zone with a porosity of 30 to 40 vol.-% (Fig.5-49 of Nagra (2024e)).

Due to the limited dataset (one hydraulic packer test available in the Benken borehole), the same set of parameters were attributed to the anhydrite-rich units of the Keuper (AAK, MAK and DAK). This is motivated by the swelling capacity carried by the transformation of the anhydrite into gypsum that is expected to prevent the formation of conductive brittle structures.

Faults in rocks with clay-mineral contents between 20 and 40 wt.%

Fault transmissivities in the SCAD unit were estimated based on the dataset of fault rock permeabilities presented by Jolley et al. (2007). Considering hydraulic conductivities up to 10^{-9} m/s and a thickness of the fault rock of 10 cm (Section 4.7.2 of Nagra 2014b), a best estimate of 10^{-10} m^2/s is calculated. The upper bound is set one order of magnitude higher.

Due to the lack of specific data, the marly units MM, MM1 and MM2 were parametrised equally.

The SK unit (Sandy Keuper) is characterised by a high quartz and feldspar content. Fault transmissivity could be enhanced, and therefore the upper bound was chosen identical (1×10^{-5} m^2/s) as in the carbonate-rich aquifers (e.g. Malm aquifer).

5.3.4 Lateral hydraulic gradients in aquifers

Lateral hydraulic gradients in the aquifer units of the Malm, Hauptrogenstein, Keuper (JO-DK, ZNO-DSK and SK units), and Muschelkalk were derived from site-specific borehole hydraulic head data (Tab. 5-1, Encl. 7-1), or based solely on the simulated potentiometry of aquifers from available stationary groundwater flow models (e.g. Nagra 2024f, Gmünder et al. 2014) in the case of a lack of field data (e.g. Hauptrogenstein aquifer).

The results of alternative cases from older models (Gmünder et al. 2014) were considered to fix the upper and lower bounds. A factor of 2 to 5 typically separates the bounds and the best estimate. Information regarding the regional groundwater flow patterns of the considered aquifers (e.g. the locations of the infiltration and exfiltration areas) is provided in Section 4.5.4 of Nagra (2024e).

Malm aquifer

For the NL and ZNO siting regions, the best estimate is set equally to 1×10^{-2} m/m. While the lateral gradient is oriented towards the west/northwest in ZNO (i.e. discharge area located along the Rhine River in the Rhine Falls and Rheinau areas), groundwater flow in NL is oriented approximately towards the north (i.e. exfiltration zones in the Rhine Valley in the region of Kaiserstuhl – Hohentengen).

Hauptrogenstein aquifer

Due to lack of field data, lateral hydraulic gradients in the Hauptrogenstein aquifer were estimated based on the results of the various available groundwater flow models (best estimate: 5×10^{-2} m/m). The recharge mainly occurs on the topographic high north of the JO siting region where the Hauptrogenstein is outcropping. The potential discharge areas are located along the Aare River to the east, assuming that the transmissive facies reach the lower Aare Valley, and in the Sissle Valley to the west.

Keuper aquifer: JO-DK, ZNO-DSK and SK

In the ZNO siting region, the best estimate of the lateral gradient is set to 5×10^{-2} m/m. The groundwater flow is approximately directed towards the south/southeast.

In the NL siting region, a lateral hydraulic gradient of 5×10^{-2} m/m, oriented southward was inferred based on borehole data.

A best estimate of 1×10^{-3} m/m is calculated for the JO siting region. While the recharge occurs along the outcrops north of the site, potential discharge areas are located along the Aare River to the east and in the Sissle Valley to the west. The groundwater flow direction in the JO siting region likely depends on the extension of the transmissive facies of the Keuper aquifer towards the east.

Muschelkalk aquifer

A lateral gradient of 1×10^{-3} m/m is derived for the NL siting region. The groundwater flow is oriented towards the west, that is toward the discharge area at the convergence of the Rhine and Aare Rivers.

A higher lateral gradient of 1×10^{-2} m/m was inferred for the ZNO siting region. The groundwater flow is oriented towards the southwest.

In the JO siting region, the best estimate of 5×10^{-3} m/m is between the values of NL and ZNO, and groundwater flow is developing towards the east (i.e. towards the exfiltration zones located in the Klingnau Lake area). Another groundwater flow system exists in the western part of JO, with flow directed towards the Sissle River.

5.3.5 Hydraulic heads and vertical gradients in the Opalinus Clay

Hydraulic heads in the Opalinus Clay and vertical gradients across this unit can be described under steady state conditions as well as under transient conditions (i.e. based on the LTM observations).

An example for short-term transient processes is the disturbance of the formation due to the drilling and testing activities days or weeks after drilling (Section 5.6.5 of Nagra 2024e). Due to the low hydraulic diffusivity of the Opalinus Clay, transient processes can also persist over much longer time periods. The measured hydraulic heads in Opalinus Clay in long-term monitoring (LTM) systems indicates underpressures (with respect to hydrostatic) and may be interpreted to reflect a response to unloading from exhumation or glacial cycles over several thousand years (Section 5.6.5 of Nagra 2024e).

The aquifers located above and below the host rock and confining units act as the hydraulic boundary conditions of the aquitard system. They exert a strong control on the steady-state profile of hydraulic heads in these low permeable units toward which the transient hydraulic heads are continuously evolving.

In the following, it is discussed how the measured underpressures can be considered as lower bound (Section 5.3.5.1), and extrapolation of the steady-state conditions across the bounding aquifers as upper bound in Opalinus Clay (Section 5.3.5.2).

5.3.5.1 Lower bound

(defined based on transient conditions)

The LTM in Benken represents the most developed hydraulic head profile compared to the newly equipped boreholes (Nagra 2024e) as it has been in operation since July 2009. It is therefore considered the most reliable dataset for the estimation of the formation hydraulic head. Note that a trend to anomalous underpressure is also visible in the newly installed LTMs (Nagra 2024e).

Hydraulic head

In ZNO, the lower bound (330 m a.s.l.) is based on the lowest hydraulic head measured in the Opalinus Clay of the Benken borehole, that is about 70 m lower than the altitude of the ground surface. Such a magnitude of underpressure may be related to unloading from erosion and glacial cycles in the Quaternary (Section 5.6.5 of Nagra 2024e).

Since the NL siting region experienced a similar recent geologic history as ZNO (Chapter 6 of Nagra 2024eNagra), the same lower bound (330 m a.s.l) was chosen also for the NL siting region. This value is higher than the hydraulic head measured in the long-term monitoring interval in the «Herrenwis Unit» of the STA3 borehole. The latter value was not used for the definition of the lower bound for the following reasons:

- The hydraulic head measured in the STA3 intervals in the Opalinus Clay and the overlying Wedelsandstein Formation (i.e. between the Opalinus Clay and the «Herrenwis Unit») are >330 m a.s.l. (status 1.5.2024).
- The measurement intervals in the Opalinus Clay of the STA3 borehole show a time evolution of the hydraulic head that is consistent with the ones observed in the measurement systems of BEN and MAR1.

In the JO siting region, the hydrogeological system is interpreted to be strongly influenced by topography of the Bözberg plateau. The altitude of the ground surface is therefore not considered as a good proxy for hydrostatic conditions. Instead, the well-defined hydraulic heads measured in the Muschelkalk aquifer in the boreholes of the JO siting regions (i.e. 383 to 396 m a.s.l.) were used as a reference for the determination of the lower bound. A value of 300 m a.s.l., which is approximately 80 to 100 m below the reference hydraulic heads, was chosen.

Vertical hydraulic gradient

The vertical hydraulic head distribution from the LTM of the BEN borehole in the ZNO siting region shows that the vertical hydraulic gradients are oriented towards the Opalinus Clay (Fig. 5-6). It follows that the net vertical flux across the Opalinus Clay is null. This was conceptually quantified as a net 0 vertical hydraulic gradient.

This concept was further considered for the other siting regions (JO and NL) since a trend to underpressure is also observed in the Opalinus Clay in the newly installed systems (Section 5.6.5 of Nagra 2024e).

5.3.5.2 Upper bound

(defined based on steady-state conditions in bounding aquifers)

Large-scale hydraulic head differences between the aquifers above and below the host rock define the steady state hydraulic head profile towards which the aquitard system is continuously evolving. The resulting vertical hydraulic gradients in the host rock and confining units give information on the transport dynamics in the aquitard system under steady state hydraulic conditions.

Hydraulic head

The applied methodology involves the estimation of a representative steady state hydraulic head in the host rock by linearly interpolating the hydraulic head between adjacent aquifers using borehole data. The highest interpolated value was used to set the upper bound if artesian conditions prevail. Otherwise, the upper bound was set to a representative topographic elevation (i.e. altitude of the ground surface).

Following this approach, an upper bound of 440 m a.s.l. was considered for the ZNO siting region as a result of the artesian conditions occurring in the Keuper aquifer of the Benken borehole (Fig. 5-6). The upper bound of the hydraulic head in the NL siting region was set to a representative topographic elevation of 410 m a.s.l. since all aquifers display non artesian conditions.

In the JO siting region, the determination of a representative topographic elevation is not evident due to the hilly topographic situation. The upper bound (460 m a.s.l.) is thus defined based on the maximal steady state hydraulic heads in the host rock inferred using TBO and LTM data.

Vertical hydraulic gradients

Stationary vertical hydraulic gradients across the Opalinus Clay are estimated for each siting region by calculating the large-scale steady state vertical hydraulic gradients between adjacent aquifers (i.e. the difference in hydraulic head divided by the distance between the considered aquifers) using borehole data. The values are supplemented by the stationary hydraulic gradients calculated from the various available stationary groundwater flow models. The upper bounds provided in Encl. 7 consist of absolute magnitudes of the stationary vertical hydraulic gradients. Indication on their direction is given in the text below.

The steady state vertical hydraulic gradients across the Opalinus Clay are oriented upward in the ZNO siting region because of the high hydraulic heads of the Keuper aquifer (i.e. Benken borehole), and the comparatively lower hydraulic heads in the Malm aquifer that are strongly controlled by the outcrops along nearby Rhine River. A value of 0.5 m/m was chosen as an upper bound based on the different datasets.

In the JO siting region, the recharge of the Hauptrogenstein aquifer through outcrops along the northern border of the siting region leads to high hydraulic heads in this aquifer. This translates into the dominance of downward hydraulic gradients. Due to the topographic and outcrop situations, a stationary vertical hydraulic gradient of 1 m/m was used for the upper bound.

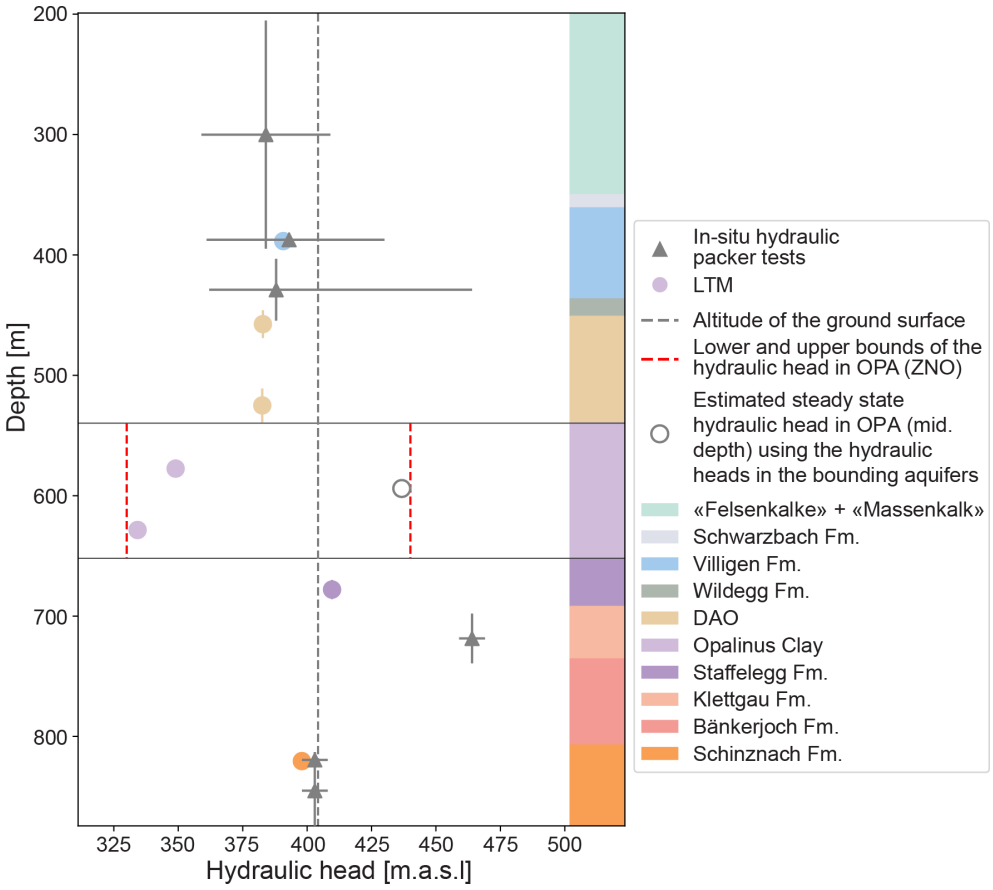

Fig. 5-6: Hydraulic head measurements and recommended bounds in the BEN borehole

Circles in colour reflect data points from the long-term monitoring system (LTM; status 01.05.2024). Results from the packer tests (grey triangles) are only shown for the aquifers to highlight good match between short-term and long-term measurements of the LTM. DAO: Dogger Group above Opalinus Clay.

The NL siting region shows a more complex situation that mainly reflects the local dynamic of the Malm aquifer and the intermittent presence of the Keuper aquifer. Downard hydraulic gradients prevail in the southern part of the siting region reflecting notably the recharge of the aquifer occurring north of the Jura Main Overthrust. Stationary hydraulic gradients are oriented upward in the northern part of the siting region. A representative stationary vertical hydraulic gradient of 0.5 (valid in both vertical directions) is inferred based on the considered datasets.

6 Geomechanical properties

6.1 Introduction

Geomechanical properties and the effective stress magnitudes control the deformation behaviour of the rock mass. For a deep geological repository, this is of relevance for the following aspects:

- Long-term stability and repository layout (acceptable thermally-induced-fluid or gas pressures in the Opalinus Clay)
- Construction of access and underground structures (Opalinus Clay and overlying formations)

A detailed evaluation of the site-specific stress field, including estimates of depth-dependent stress magnitudes in Opalinus Clay and in overlying formations along potential access structures is provided in Nagra (2024j).

Key geomechanical properties relevant for engineering design and construction planning have been summarised in the Bautechnische Dossiers (Nagra 2023a, 2023b, 2023c).

This chapter provides additional conceptual considerations relevant for the derivation of the recommended geomechanical properties and provides unit-specific parameter bandwiths.

6.2 Database

The geomechanical parameter groups including data sources are listed in Tab. 6-1.

Tab. 6-1: List of geomechanical parameter groups and respective data sources.

The Dossier numbers refer to the TBO reports listed in Tab. 1-1. *Only for BOZ1, BOZ2, STA2 and STA3 boreholes.

Parameter group	Primary data	Complementary data
Geomechanical properties of Opalinus Clay	Laboratory tests (TBO Dossier IX, Crisci et al. 2024b Pressuremeter tests in situ (TBO Dossier VI*, Elkhoury et al. 2022, Elkhoury et al. 2024)	Geophysical logs (TBO Dossier VI) MultiMin (Becker & Marnat 2024) Isotropic compression tests (Braun et al. 2025) Comparison of laboratory tests and pressuremeter tests at Mont Terri URL (Liu et al. 2022)
Geomechanical properties of other formations	Laboratory tests (TBO Dossier IX)	Geophysical logs (TBO Dossier VI)

6.3 Conceptual considerations to derive parameter bandwidths

6.3.1 Geomechanical properties of the Opalinus Clay

The general deformation behaviour of Opalinus Clay is summarised in Section 5.5 of Nagra (2024e). Different constitutive models and numerical codes are used to account for various aspects of the complex material behavior depending on the aims of investigation. For construction design and tunnel-static analyses this is specified in Section 3.3.1 of Nagra (2023d), and for scoping calculations concerning the long-term evolution of thermal and gas pressures details can be found in Chapter 3 of Nagra (2024g) and Chapter 4 of Nagra (2024h). The different constitutive models use different parametrisations, and it is not possible to provide universally valid hydro-mechanical properties. Therefore, the recommended material parameters in Encl. 6-1 may deviate from modelling parameters used in specific scoping calculations.

The key dataset for hydromechanical property assignment of Opalinus Clay is documented and discussed in Crisci et al. (2024b). Assuming a Mohr-Coulomb-type failure envelope, effective cohesion values and friction angles are derived from more than 140 tests. In the same reference, it is also argued that Opalinus Clay was tested in a representative way, both with respect to material variability within the formation, and number of tests across the different siting regions and source depths. Samples sourced from more shallow depth (400 to 700 m) exhibit slightly higher porosity and lower peak strength when loaded perpendicular to bedding than samples sourced from greater depth (700 to 900 m), but this difference is negligible compared to the overall variability of the material and was not observed in other loading directions. In terms of geomechanical properties, the Opalinus Clay can therefore be considered as the “same material” in all three siting regions. However, both strength and stiffness are dependent on effective stress. For strength parameters, this is accounted for by the Mohr-Coulomb effective cohesion and friction parameters, and for undrained E-moduli this is accounted for by two different effective stress intervals (Encl. 6-1).

Also included in the parameter bandwidth of Encl. 6-1 is the drained bulk modulus (K_d). The quantification of this parameter is based on the triaxial test results of the TBO campaign, in particular: (i) the isotropic unloading (reverse consolidation) data prior to shearing was used to measure K_d, and (ii) the K_d values were also calculated from the elastic properties during the drained shear phase, adopting a cross-anisotropic formulation. All results (measured and calculated) showed that K_d values range between 2 and 7 GPa, with a best guess of approximately 4 GPa, in the confining stress range of 5 – 15 MPa. A similar range of values was also obtained by complementary drained tests of STA3 core material with Opalinus Clay conducted in an isotropic compression cell at ParisTech (Braun et al. 2025).

The laboratory tests exhibit only a small variability in strength, despite relatively large variability in bulk mineralogy (clay-mineral content ranging from 32 to 71 wt.%). This can be explained by the clay-matrix dominating the microstructure for nearly the entire spectrum of the mineralogical variability (Fig.5-57 of Nagra (2024e)), with some exceptions discussed further below. Not addressed in Crisci et al. (2024b) is the scaling of rock properties to rock mass properties. This involves two aspects, (i) the scale-dependent material variability, and (ii) the tectonic overprint in situ, and those aspects are discussed separately in the following subsections.

Scale-dependent material variability

In the laboratory, tested sample cylinders are only 38 to 50 mm long. The variability at this scale is larger than that at the metre scale, typical for underground structures. Yet the variability in strength of the test results is also small with equivalent unconfined compressive strengths in the range of 21 ± 5 MPa (Crisci et al. 2024b). A somewhat larger scatter is observed for stiffness (undrained E-moduli), although this can partly be attributed to differences in the amount of strain

used to compute this parameter. The largest deviation from the mean stiffness (up to a factor two from the mean trend) is observed for a few test samples with unusual mineralogy for Opalinus Clay, with lower clay-mineral content (<40 wt.%), and high quartz or calcite content (>20 wt.%). The slight difference in strength and stiffness of these facies compared to Opalinus Clay with clay-mineral content >40 wt.% is attributed to a more dominant contribution of diagenetic cement or a grain-supported microstructure as has been proposed also for Opalinus Clay at the Mont Terri rock laboratory (Crisci et al. 2021).

However, it can be shown that intervals with unusually low clay-mineral content in Opalinus Clay are i) very rare even at the scale of geophysical logging (approximately 15 – 20 cm) and ii) are distributed in the upper or uppermost part of the formation (Fig. 6-1). Given the scarcity in occurrence and distribution, the impact of such intercalations of lower clay-mineral content are on the overall geomechanical behaviour of the rock mass is considered negligible. Therefore, the measurements of samples with lower clay-mineral content were not fully included in the parameter bandwidth of Encl. 6-1 (Crisci et al. 2021).

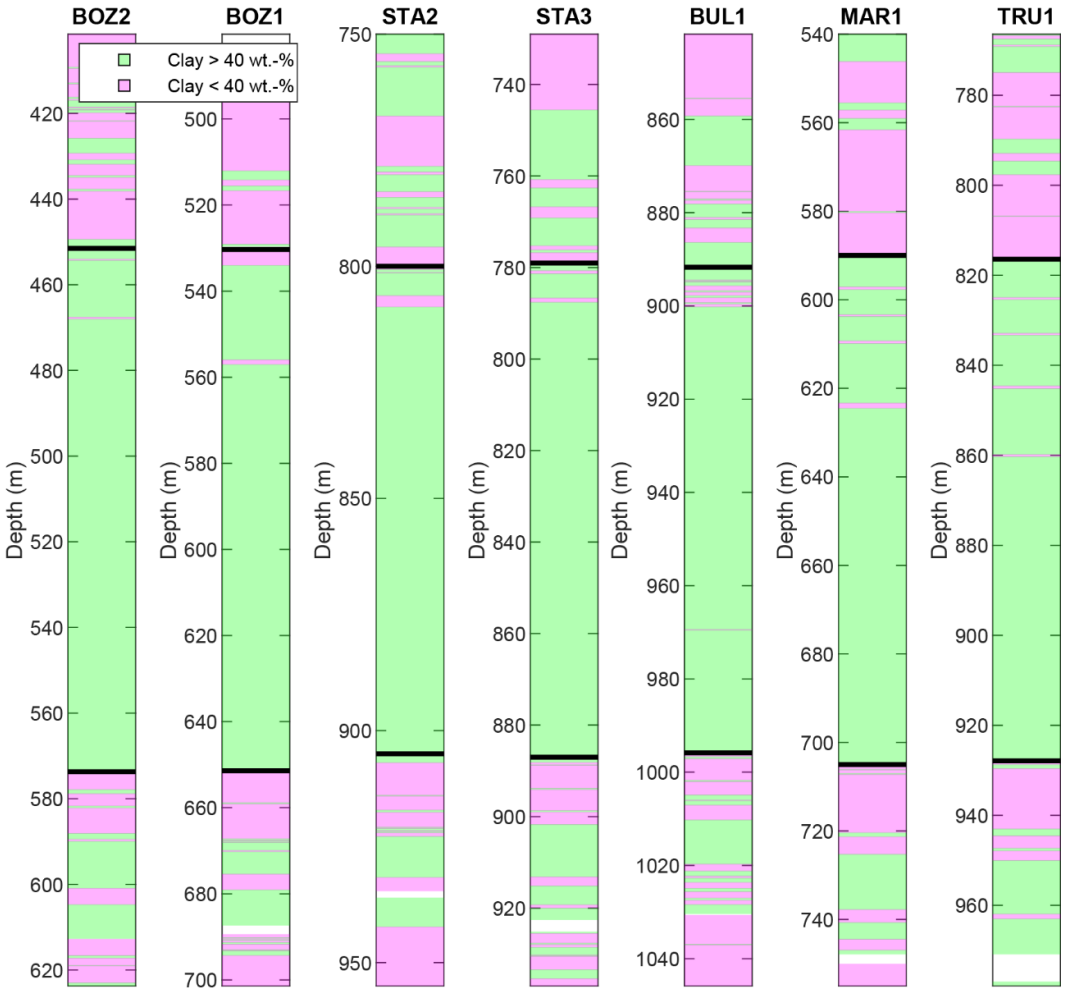

Fig. 6-1: Distribution of geomechanically different facies in Opalinus Clay and adjacent confining units

Top and base of the Opalinus Clay interval in the various boreholes is delimited with solid black lines. Clay-dominated facies (Green): clay-mineral content >40 wt.%; quartz- or calcite-rich facies (Purple): clay-mineral content <40 wt.%. Plots are based on MultiMin results (Becker & Marnat 2024).

Potential scaling effects on geomechanical properties were also actively explored by pressuremeter testing (PMT) in the borehole (Tab. 6-1). In this test a packer with an effective contact length of 50 to 100 cm is inflated and deflated in cycles, thereby loading the borehole wall. At the Mont Terri rock laboratory, this was performed with high-resolution strain gauges to measure deformation (Liu et al. 2022), and in the TBO this was done with a packer on wireline formation testing tool (Elkhoury et al. 2022, Elkhoury et al. 2024). In both cases the field test results in situ were compared to laboratory test results with cores from either the same or immediately adjacent intervals, and representative samples for the laboratory test results were chosen based on X-ray CT scans and sonic logs. Since packer inflation during PMT corresponds to cavity loading, the shear modulus is the best suited elastic parameter to compare directly to laboratory tests.

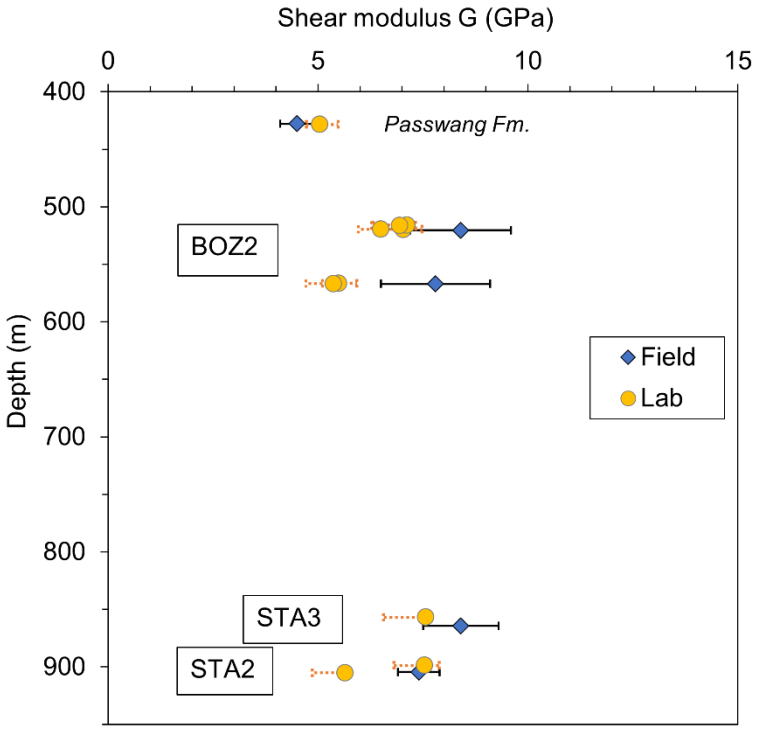

Fig. 6-2: Comparison of shear moduli derived from field (PMT) and laboratory test results

All tests are in Opalinus Clay except for the test indicated (Passwang Formation).

A comparison of test results from the TBO campaign is provided in Fig. 6-2. Overall, the agreement is good, with the larger-scale PMT results tending to slightly higher values. The possible causes for the small but rather systematic difference between lab tests and PMT are discussed in more detail in (Elkhoury et al. 2024). The difference is not considered to be associated with damage of laboratory testing specimens from core extraction and sample preparation. Where such damage occurred, it was possible to identify this diagnostically and as outliers when test results were plotted as a function of basic properties (Dossier IX of Nagra (ed.) 2022a and 2022b, Crisci et al. 2024a). Instead, the small difference in shear moduli can be attributed to different strains in laboratory and field tests (Liu et al. 2022, Elkhoury et al. 2024).

Taking the strain-dependence into consideration, the agreement between laboratory tests and the field tests is excellent and provides confidence that rock properties from laboratory samples can indeed be used to bracket the intact rock mass at a larger scale.

Tectonic overprint

Fracture frequency in Opalinus Clay is low, often with continuous core of several metres in length essentially free of natural discontinuities, with some clusters of higher frequencies (Nagra 2024e). In addition, many of the existing fractures are mineralised and do not represent effective planes of weakness. But smaller (sub-seismic) faults are present in Opalinus Clay and this needs to be accounted for in quantitative scoping calculations.

The evolution of shear strength during fracturing was studied in detail in triaxial tests (Crisci et al. 2024b). The large data volume highlighted that fracturing is associated with a loss of effective cohesion, with only minor changes to the effective friction angle. Fractured Opalinus Clay intervals may therefore be approximated with post-peak strength values as constrained from triaxial testing (post-peak effective cohesion and friction values in Encl. 7-1).

In faults with larger shear displacements, the approximation by parameters from triaxial testing may not be appropriate, as such tests are limited to shear displacements of a few millimetres. Complementary tests were therefore done to mimic fault gouge material expected at larger displacements. To this end, intact Opalinus Clay was crushed, remoulded and recompacted. In addition to triaxial tests of such recompacted Opalinus Clay, samples were also tested to much larger strain in a ring shear apparatus. These investigations yielded lower bounds for the friction angle between 10° and 17° for different facies, i.e. for high and low clay-mineral contents (Ferrari et al. 2020). Whereas the latter is broadly consistent with the 20° as lower bound for post-peak frictional strength in the conventional triaxial tests, the 10° are significantly lower. But the remoulded tests were done with distilled water and by removing larger grains from the crushed Opalinus Clay to explore the theoretical lower bounds of shear strength. Elimination of larger grains changes the structure of the material, altering the interlocking and creating a rather smooth shearing surface. It is also noted that no such gouge material was encountered in the TBO in the Opalinus Clay. Real clay-rich gouge material from the main fault at Mont Terri yielded friction coefficients of approximately 0.3 (Orellana et al. 2018), which corresponds to 17°, hence also much higher than the 10°.

The fault architecture in Opalinus Clay can be described as strongly heterogeneous and segmented (see Section 5.5 in Nagra 2024e), without strong localisation along planes filled with gouge material over distances of tens of metres. In combination with the above considerations, a lower bound of 20° with zero effective cohesion is therefore considered appropriate for the expected size of faults in Opalinus Clay at the siting regions.

6.3.2 Geomechanical properties of over- and underlying formations

For formations other than Opalinus Clay, the lithological and mechanical variability is generally larger and laboratory testing frequency much lower. For this reason, geophysical logging was used in combination with laboratory tests to estimate the value range of elastic and strength parameters. This semi-empirical approach is customary for property assignment in reservoir models (e.g. Tutuncu et al. 1998) and widely used in the hydrocarbon industry. Using this approach, continuous "dynamic" elastic properties are first derived along the boreholes from wave velocities (sonic scanner) in combination with bulk density.

For isotropic materials, the dynamic Young's modulus (E_{dyn}) can be expressed as functions of P- and S-wave velocities (V_p and V_s, respectively) and bulk density ρ:

$$E_{dyn} = \rho V_s^2 \frac{3{V_p}^2 - 4{V_s}^2}{V_p^2 - V_s^2} \qquad \textit{Eq. 6.1}$$

On the other hand, “static” elastic properties are derived from laboratory testing with small increments in static loading, that is the slope of the stress-strain curve.

For the static Young's modulus (E_{stat}), this is the increment of axial stress versus the increment in axial strain:

$$E_{stat} = \frac{\Delta\sigma_a}{\Delta\varepsilon_a} \qquad \textit{Eq. 6.2}$$

For clay rocks, dynamic Young's moduli are generally larger than static moduli (Fjær 2019), and this was also explored as a function of the clay-mineral content in selected samples of the TRU1 borehole (Mews et al. 2024). Therefore, the dynamic values need to be “calibrated” on the static values from laboratory tests.

The correlation between static and dynamic values can thus be expressed as:

$$E_{stat} = \mathrm{d}_E E_{dyn} \qquad \textit{Eq. 6.3}$$

where d_E, the correlation factor, depends on rock type and was established for each formation separately and interpolatedd where no laboratory data was available. Anisotropy was considered by assuming a transverse isotropy, calibrating logs to the appropriate lab measurements (loading perpendicular and parallel to bedding, respectively) and using Gamma-ray log (GR) results for scaling of anisotropy (generally higher anisotropy with higher GR values).

An example of the workflow to derive the parameter bandwidth for elastic moduli in the direction vertical to bedding is illustrated in Fig. 6-3. The continuous blue line in Fig. 6-3a depicts the E_{dyn} values according to *Eq. 6-1* but already includes the shift (from calibration) to the static values of the laboratory tests (shown in Orange) using the formation-specific correlation factor for «Felsenkalke» + «Massenkalk». The continuous curve consists of points at a spacing of approximately 15 – 20 cm along the boreholes. These points define a cumulative distribution (Fig. 6-3b), with the laboratory values shown for comparison and arbitrarily plotted at the P0.05 and P0.10 (probability) level. The statistical values of the parameter bandwidth are then constrained from the distribution curve (Fig. 6-3c).

The above workflow was also applied to Poisson's ratio and unconfined compressive strength (UCS). The resulting data is graphically illustrated in Enclosures 6-1a to 6-1c and tabulated in sheet 6-2 in Encl. 7-1.

Not included in the graphics and tables are values for the Opalinus Clay, as these were constrained in much more detail from laboratory and field analysis (see Section 6.3.1 and sheet 6-1 of Encl. 7-1). But mechanical properties of Opalinus Clay were also constrained by the combined laboratory test and logging workflow as explained above and used as input for geomechanical-numerical stress modelling and can be found in Chapter 4 of Nagra (2024j). This was done to ensure a coherent set of data (cumulative distribution) with plausible stiffness contrasts across formations.

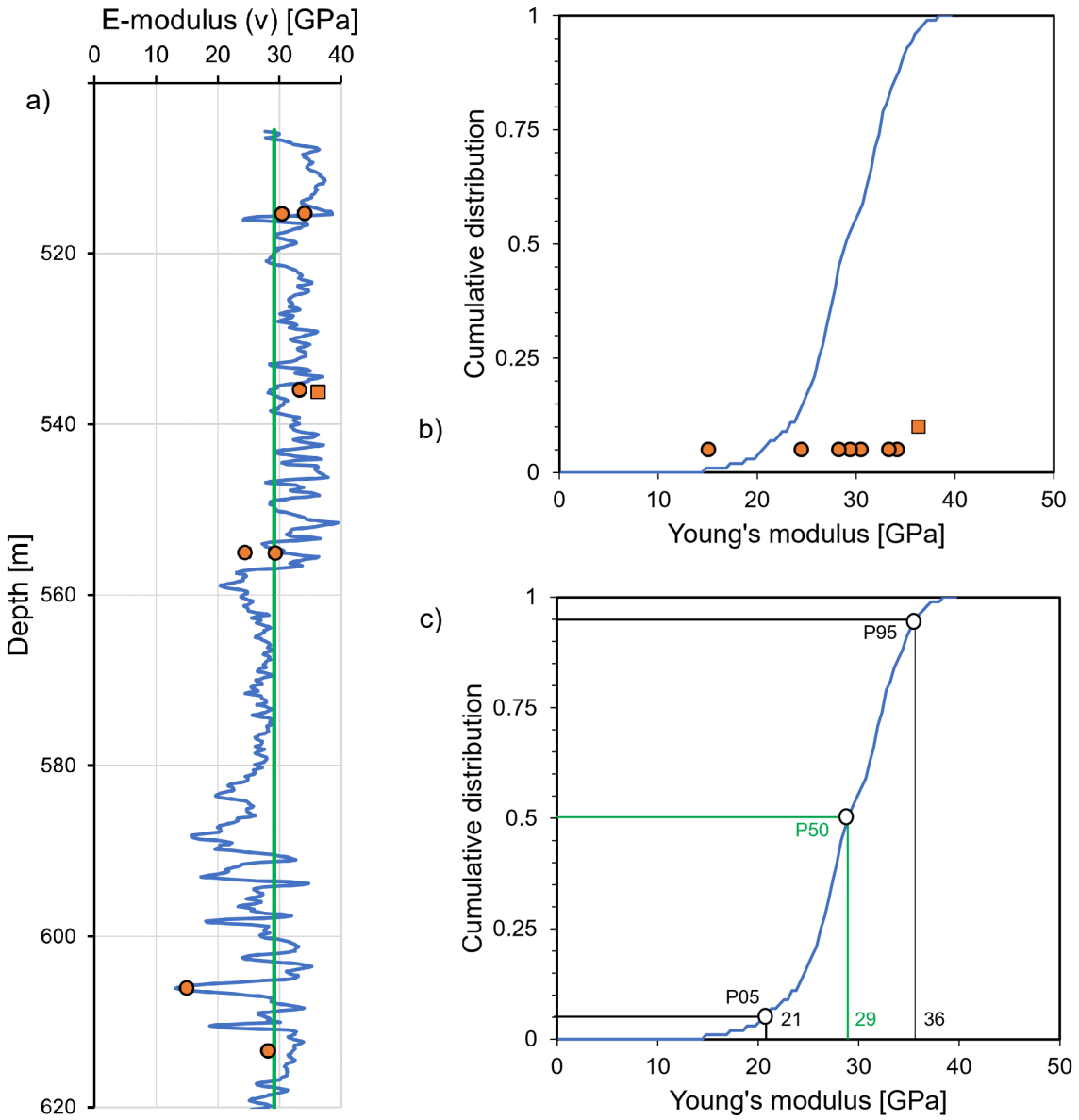

Fig. 6-3: Example of empirical correlation of geophysical log and lab results

Example is for intervall «Felsenkalke» + «Massenkalk» of the TRU1 borehole. a) Orange circles and square depict laboratory test results (unconfined compressive strength, UCS tests, and triaxial, TRX test, respectively), Blue line represents continuous dynamic Young's moduli after correlation with the static Young's moduli of lab tests. b) Cumulative distribution curve of entire formation compared to laboratory test results. c) Statistical values of the distribution curve with median value (P50) of approximately 29 GPa, as also indicated by the vertical green line in (a).

7 Summary

The geology of the three siting regions was simplified and abstracted for the purpose of quantitative site comparison and numerical analyses such as performance assessment and dose calculations.

The abstraction of the geology defines units with similar properties (Encl. 2), and the 3D stratification of these abstracted units is documented as depth- and thickness maps (Encl. 3). The extent of the maps in the respective siting regions delineate the area of interest containing the potential repository zone.

For each abstracted unit, key properties relevant for transport and mechanical stability are synthesised (Encl. 4 to 6).

Complemented with conceptual arguments, recommended bandwidths for these key properties are provided in Encl. 7-1., covering the following parameters for the abstracted units in separate sheets:

- Unit thickness as measured in the boreholes (sheet 2_2)
- Clay-mineral content (sheet 4_1)
- Porosity and grain density (sheets 4_2 and 4_3)
- Hydraulic conductivity of the rock mass and fault transmissivity (sheet 5_1)
- Horizontal gradients in aquifers (sheet 5_2)
- Vertical hydraulic gradients and heads in Opalinus Clay (sheets 5_3 and 5_4)
- Geomechanical properties of Opalinus Clay (sheet 6_1)
- Rock mechanical properties of other abstracted units (sheet 6_2)

Data users may further simplify or adapt these units and parameters depending on the aim of investigation.

As emphasised in the introduction, the following additional key parameters are covered in separate reports:

- Stress field Nagra (2024j)
- Diffusion properties of host rock and confining units (Glaus et al. 2024)
- Sorption properties of host rock and confining units (Miron et al. 2024)
- Thermal properties and temperature conditions (Nationale Genossenschaft für die Lagerung radioaktiver Abfälle 2024l)
- Porewater chemistry of the Opalinus Clay (Mäder & Wersin 2023)

For Opalinus Clay, the significantly expanded database confirms the expected thickness and barrier properties in all siting regions. The porewater chemistry and geomechanical properties are now much better constrained than in Stage 2 of the Sectoral Plan Deep Geological Repositories (SGT). Also, the spatial correlation and hydro-mechanical characterisation of the confining units is substantially improved. compared to the previous stage. A comparison of key learnings and developments of the database compared to previous investigations can be found in Section 7.1 of the geosynthesis report (Nagra 2024e).

8 References

Bauer, H., Schröckenfuchs, T. & Decker, K. (2016): Hydrogeological properties of fault zones in a karstified carbonate aquifer (Northern Calcareous Alps, Austria). Hydrogeology Journal 24/5, 1147-1170. DOI: 10.1007/s10040-016-1388-9.

Beauheim, R.L. (2013): Hydraulic conductivity and head distributions in the host rock formations of the proposed siting regions. Nagra Arbeitsbericht NAB 13-13.

Becker, J. & Marnat, S. (2024): Petrophysical Data and Core-Calibrated Multimineral Interpretation. Nagra Arbeitsbericht NAB 24-17.

Bläsi, H.R., Deplazes, G., Schnellmann, M. & Traber, D. (2013): Sedimentologie und Stratigraphie des 'Brauner Doggers' und seiner westlichen Äquivalente. Nagra Arbeitsbericht NAB 12-51.

Braun, P., Alavoine, A., Ghabezloo, S., Delage, P. & Giger, S.B. (2025): Poromechanical behaviour of a deep shale core for geological radioactive waste storage. Rock Mechanics and Rock Engineering. DOI: 10.1007/s00603-025-04382-2.

Childs, C., Manzocchi, T., Walsh, J.J., Bonson, C.G., Nicol, A. & Schöpfer, M.P. (2009): A geometric model of fault zone and fault rock thickness variations. Journal of Structural Geology 31/2, 117-127. DOI: 10.1016/j.jsg.2008.08.009.

Crisci, E., Ewy, R.T., Ferrari, A., Giger, S.B., Ewy, R. & Giger, S. (2024a): Assessing swelling-induced damage in shale samples during triaxial testing. Geomechanics for Energy and the Environment 40, 100599. DOI: 10.1016/j.gete.2024.100599.

Crisci, E., Ferrari, A., Giger, S.B. & Laloui, L. (2021): Effect of the mineralogical composition on the elastoplastic hydromechanical response of Opalinus Clay shale. International Journal of Rock Mechanics & Mining Sciences 143, 104747. DOI: 10.1016/j.ijrmms.2021.104747.

Crisci, E., Giger, S.B., Laloui, L., Ferrari, A., Ewy, R., Stankovic, R., Stenebråten, J., Halvorsen, K. & Soldal, M. (2024b): Insights from an extensive triaxial testing campaign on a shale for comparative site characterization of a deep geological repository. Geomechanics for Energy and the Environment 38, 100508. DOI: 10.1016/j.gete.2023.100508.

de Marsily, G. (1986): Quantitative Hydrogeology. Groundwater Hydrology for Engineers. Academic Press, Inc., San Diego.

Eberli, G.P., Anselmetti, F.S., Kroon, D., Sato, T. & Wright, J.D. (2002): The chronostratigraphic significance of seismic reflections along the Bahamas Transect. Marine Geology 185/1-2, 1-17. DOI: 10.1016/S0025-3227(01)00287-0.

Elkhoury, J.E., Bérard, T., Desroches, J., Peyret, E., Prioul, R., Crisci, E., Garrard, R. & Giger, S.B. (2024): In situ static elastic properties assessment and validation with pressuremeter testing using a formation tester tool. Geomechanics for Energy and the Environment 40. DOI: 10.1016/j.gete.2024.100619.

Elkhoury, J.E., Elias, Q.K., Prioul, R., Peyret, E., Wilcox, A., Di Giovanni, M., van der Hulst, T., Bérard, T., Desroches, J., Garrard, R. & Giger, S.B. (2022): The First Pressuremeter Testing Campaign on Wireline Formation Testers in Deep Boreholes. ARMA 22-0698. 56th US Rock Mechanics/Geomechanics Symposium, Santa Fe, NM, USA, 26-29 June 2022.

Ferrari, A., Rosone, M., Ziccarelli, M. & Giger, S.B. (2020): The shear strength of Opalinus Clay shale in the remoulded state. Geomechanics for Energy and the Environment 21, 100142. DOI: 10.1016/j.gete.2019.100142.

Fisher, Q.J., Haneef, J., Grattoni, C.A., Allshorn, S. & Lorinczi, P. (2018): Permeability of fault rocks in siliciclastic reservoirs: Recent advances. Marine and Petroleum Geology 91, 29-42. DOI: 10.1016/j.marpetgeo.2017.12.019.

Fisher, Q.J. & Knipe, R.J. (1998): Fault sealing processes in siliciclastic sediments. Geological Society, London, Special Publications 147, 117-134. DOI: 10.1144/ GSL.SP.1998.147.01.08.

Fjær, E. (2019): Relations between static and dynamic moduli of sedimentary rocks. Geophysical Prospecting 67/1, 128-139. DOI: 10.1111/1365-2478.12711.

Freeze, R.A. & Cherry, J.A. (1979): Groundwater. Prentice-Hall Inc., Englewood Cliffs.

Glaus, M.A., Kulik, D.A., Miron, G.D., Van Loon, L.R., Wüst, R., Becker, J. & Li, X. (2024): Diffusion Databases for Opalinus Clay, Confining Geological Units and Bentonite: Methods, Concepts and Upscaling of Data. Nagra Technical Report NTB 23-08.

Gmünder, C., Malaguerra, F., Nusch, S. & Traber, D. (2014): Regional Hydrogeological Model of Northern Switzerland. Nagra Arbeitsbericht NAB 13-23.

Jolley, S.J., Dijk, H., Lamens, J.H., Fisher, Q.J., Manzocchi, T., Eikmans, H. & Huang, Y. (2007): Faulting and fault sealing in production simulation models: Brent Province, northern North Sea. Petroleum Geoscience 13/4, 321-340. DOI: 10.1144/1354-079306-733.

Liu, L., Giger, S.B., Martin, D., Chalaturnyk, R., Schuster, K., Deisman, N. & Keller, L. (2022): In-situ shear modulus determination by pressuremeter tests in Opalinus Clay and reconciliation with laboratory tests. Rock Mechanics and Rock Engineering 55/8, 4615-4635. DOI: 10.1007/s00603-022-02873-0.

Longridge, D., Vogt, T. & Pechstein, A. (2024): Datenbericht Langzeitbeobachtung Benken, Marthalen-1-1, Bözberg-1-1, Stadel-3-1: Dokumentation der Messdaten 2022. Nagra Arbeitsbericht NAB 23-35.

Mäder, U. & Wersin, P. (2023): Reference porewaters for SGT Stage 3 of the Opalinus Clay for the siting regions Jura Ost (JO), Nördlich Lägern (NL) and Zürich Nordost (ZNO). Nagra Arbeitsbericht NAB 22-47.

Mews, K.S., Lozovyi, S., Stenebråten, J.F., Giger, S.B. & Holt, R.M. (2024): Experimental study of seismic dispersion: influence of clay mineral content. Geophysical Journal International 236/3, 1545-1566. DOI: 10.1093/gji/ggad500.

Miron, G.D., Marques Fernandes, M., Kulik, D.A., Marinich, O., Baeyens, B., Wüst, R., Becker, J. & Li, X. (2024): Sorption Databases for Opalinus Clay, Confining Geological Units and Bentonite: Methods, Concepts and Upscaling of Data. Nagra Technical Report NTB 23-06.

Nagra (1992): Sondierbohrung Siblingen Untersuchungsbericht: Textband und Beilagenband. Nagra Technischer Bericht NTB 90-34 A & B.

Nagra (2010): Beurteilung der geologischen Unterlagen für die provisorischen Sicherheitsanalysen in SGT Etappe 2 - Klärung der Notwendigkeit ergänzender geologischer Untersuchungen. Nagra Technischer Bericht NTB 10-01.

Nagra (2014a): SGT Etappe 2: Vorschlag weiter zu untersuchender geologischer Standortgebiete mit zugehörigen Standortarealen für die Oberflächenanlage: Geologische Grundlagen Dossier IV Geomechanische Unterlagen. Nagra Technischer Bericht NTB 14-02 Dossier IV.

Nagra (2014b): SGT Etappe 2: Vorschlag weiter zu untersuchender geologischer Standortgebiete mit zugehörigen Standortarealen für die Oberflächenanlage: Geologische Grundlagen. Dossier VI Barriereneigenschaften der Wirt- und Rahmengesteine. Nagra Technischer Bericht NTB 14-02 Dossier VI.

Nagra (2023a): Bautechnisches Dossier – Band 2: Bautechnisch relevante Auszüge geologischer Grundlagen Jura Ost. Nagra Arbeitsbericht NAB 23-01 Band 2.

Nagra (2023b): Bautechnisches Dossier – Band 3: Bautechnisch relevante Auszüge geologischer Grundlagen Nördlich Lägern. Nagra Arbeitsbericht NAB 23-01 Band 3.

Nagra (2023c): Bautechnisches Dossier – Band 4: Bautechnisch relevante Auszüge geologischer Grundlagen Zürich Nordost. Nagra Arbeitsbericht NAB 23-01 Band 4.

Nagra (2023d): Bautechnisches Dossier Standortvergleich – Band 7: Projektbasis. Nagra Arbeitsbericht NAB 23-01 Band 7.

Nagra (2024a): 3D Seismic Interpretation of Stratigraphic Horizons and Structures in Time Domain Jura Ost. Nagra Arbeitsbericht NAB 23-17.

Nagra (2024b): 3D Seismic Interpretation of Stratigraphic Horizons and Structures in Time Domain Nördlich Lägern. Nagra Arbeitsbericht NAB 23-18.

Nagra (2024c): 3D Seismic Interpretation of Stratigraphic Horizons and Structures in Time Domain Zürich Nordost. Nagra Arbeitsbericht NAB 23-19.

Nagra (2024d): Depth Conversion of the 3D Seismic Interpretation for the Area of Interest in the Jura Ost, Nördlich Lägern and Zürich Nordost Siting Regions. Nagra Arbeitsbericht NAB 24-49.

Nagra (2024e): Geosynthesis of Northern Switzerland. Nagra Technischer Bericht NTB 24-17.

Nagra (2024f): Hydrogeological Model of Northern Switzerland. Nagra Arbeitsbericht NAB 24-16.

Nagra (2024g): Model Based Performance Assessment in Support of the Safety Assessment for a Geological Repository. Nagra Arbeitsbericht NAB 24-25.

Nagra (2024h): Production and Fate of Gases in the Geological Repository. Nagra Technical Report NTB 24-23.

Nagra (2024i): Radiological Consequence Analysis for a Deep Geological Repository in Northern Switzerland. Nagra Technical Report NTB 24-18.

Nagra (2024j): Stress Field in the Siting Regions Jura Ost, Nördlich Lägern and Zürich Nordost. Nagra Arbeitsbericht NAB 24-19.

Nagra (2024k): Synthesis of Performance Assessment of the Combined Repository in Nördlich Lägern. Nagra Technischer Bericht NTB 24-22 Rev. 1.

Nagra (2024l): Thermo-hydraulic modelling of the temperature distribution in the siting regions JO, NL and ZNO. Nagra Arbeitsbericht NAB 24-24.

Nagra (ed.) (2021a): TBO Bülach-1-1: Data Report Dossier I-XI. Nagra Arbeitsbericht NAB 20-08.

Nagra (ed.) (2021b): TBO Marthalen-1-1: Data Report Dossier I-XI. Nagra Arbeitsbericht NAB 21-20.

Nagra (ed.) (2021c): TBO Trüllikon-1-1: Data Report Dossier I-XI. Nagra Arbeitsbericht NAB 20-09.

Nagra (ed.) (2022a): TBO Bözberg-1-1: Data Report Dossier I-XI. Nagra Arbeitsbericht NAB 21-21.

Nagra (ed.) (2022b): TBO Bözberg-2-1: Data Report Dossier I-XI. Nagra Arbeitsbericht NAB 21-22.

Nagra (ed.) (2022c): TBO Stadel-2-1: Data Report Dossier I-XI. Nagra Arbeitsbericht NAB 22-02.

Nagra (ed.) (2022d): TBO Stadel-3-1: Data Report Dossier I-XI. Nagra Arbeitsbericht NAB 22-01.

Nagra (ed.) (2023a): TBO BACHS-1-1: Data Report Dossier I-XI. Nagra Arbeitsbericht NAB 22-04.

Nagra (ed.) (2023b): TBO Rheinau-1-1: Data Report Dossier I-XI. Nagra Arbeitsbericht NAB 22-03.

Orellana, L.F., Scuderi, M.M., Collettini, C. & Violay, M. (2018): Frictional Properties of Opalinus Clay: Implications for Nuclear Waste Storage. Journal of Geophysical Research: Solid Earth 123/1, 157-175. DOI: 10.1002/2017JB014931.

Pesendorfer, M. & Loew, S. (2010): Subsurface exploration and transient pressure testing from a deep tunnel in fractured and karstified limestones (Lötschberg Base Tunnel, Switzerland). International Journal of Rock Mechanics and Mining Sciences 47/1, 121-137. DOI: 10.1016/j.ijrmms.2009.09.013.

Tutuncu, A.N., Podio, A.L., Gregory, A.R. & Sharma, M.M. (1998): Nonlinear viscoelastic behavior of sedimentary rocks, Part I: Effect of frequency and strain amplitude. GEOPHYSICS 63/1, 184-194. DOI: 10.1190/1.1444311.

Vail, P.R., Todd, A.G., Sangree, J.B. & Todd, R.G. (1977): Chronostratigraphic significance of seismic reflections. *In:* Payton, C.E. (ed.): Seismic Stratigraphy — Applications to Hydrocarbon Exploration. (AAPG Memoir, 26). American Association of Petroleum Geologists, 99-116.